Effective seismic response control of buildings with sliding bearings

A. Dushimimana*ᵃ [ID] **, E. Singirankabo ᵇ, L. Kathumbiᵇ** [ID]

ᵃ *Ondokuz Mayis University, Körfez, Turkey*

ᵇ *Pan African University Institute for Sciences, Technology and Innovation, Juja, Nairobi*

*E-mail: chenkodu432 @gmail.com

Keywords: Seismic isolation, friction pendulum bearing, flat surface slider, restoring force, energy dissipation, superstructure acceleration, story drift, shear force, near and far-fault ground motion

Abstract. A complete response investigation on behavior of conventional sliding bearings applicable to seismic-isolated structures has not yet been fully realized, while use of such bearings is a common practice. A Full Structural Response Investigation (FSRI) comprising energy dissipation, bearing's effective and post-yield stiffness, displacements, story drifts, shear forces, accelerations and time instants for peak responses has been carried out on a ten-story RC building model with varied superstructure stiffness, and isolated by flat and curved surface sliders under different types of earthquakes. Disregarding some of the responses mentioned above FSRI can result in poor control of seismic isolation, since all the responses are observed to be affected by the type of earthquake and bearing's slider surface. Furthermore, the findings demonstrate that seismic isolation may not provide all desired responses, and in some situations, some responses may need to be of first priority owing to their beneficial effects.

1. Introduction

Seismic isolation is about decoupling a structure from the ground so that seismic loads cannot be transmitted to the superstructure when an earthquake occurs. Since twentieth century, seismic isolation has been adopted as a strategy and accepted design technique for protecting structures against earthquake hazards. Isolators decouple a superstructure from its substructure that is in turn resting on the ground and reduce the superstructure's natural frequency by dissipating energy from seismic load. Existing seismic isolators include mainly elastomeric and sliding bearings. The latter has greater durability feature and is more preferred for large deformations, and more attractive due to its mechanism to restore force by gravity action and ability to be designed independent of the superstructure's effective mass, hence easy to model [1–3]. Sliding bearing systems are displacement dependent for passive energy dissipation, and are based on simple principle of friction. The main advantage of these isolation systems is the possibility to control a wide range of frequencies and the maximum acceleration transmitted to the superstructure using the coefficient of friction [2–4].

The sliding bearing systems are subdivided into pure friction (PF) systems, flat surface sliding bearings and Friction Pendulum Systems (FPS). PFs are the first innovations in isolation by friction: they depend on friction coefficient with sliding occurring when excitation force exceeds the frictional force [5, 6]. PFs have been reported to be effective for buildings with no overturning moments [6]. Flat surface sliding bearings are free sliding with no restoring force, simple and economical [7–10]. Furthermore, these bearings have low coefficient of friction that ranges from 0.1 to 0.15 and less than 0.02 for unlubricated and lubricated bearings, respectively [11]. Flat sliding bearings differ from the curved surface bearings in that their restoring force is provided by adding springs in the system, while

the spherical surface provides restoring force for the curved FPS [12]. FPS were invented in order to solve the problems exhibited in pure friction systems regarding permanent displacement by provision of a restoring force mechanism [13, 14]. FPS operate based on the principle of the pendulum motion and like PF systems, they also depend on the friction coefficient [15].

Over the last years, innovations in various FPS have been developed to enable multiple performance of the bearing system in seismic isolation using curved surface bearings and identified by the number of effective pendula and sliding regimes. The first being the single FPS invented back in 1980s [16, 17]. Later on, authors in [18] modified equation of single FPS to describe a smooth transition of breakaway to minimum sliding coefficient of friction. This bearing is characterized by a single sliding surface, but it is challenged by resonance, thus rendering it ineffective for some structures as the isolated structure can collapse [14, 19, 20]. To solve this problem, double FPS was invented with two effective pendula and three sliding regimes to improve relative displacement capacity and isolator flexibility [12, 21]. Researchers in [22] modified the double FPS by developing triple FPS with three effective pendula and five sliding regimes. A significant number of researchers have additionally reported various advantages of triple FPS over double FPS such as greater strength and stiffness in response to change in displacement and velocities, increased energy dissipation capacity and adaptive behavior [22–28].The latest innovation is the quintuple friction pendulum isolator, an innovation of Lee et al. [29], with five effective pendula and nine sliding regimes. The added number of pendula as well as the sliding regimes have added advantage of adaptability, but made its behavior too complex to model [29]. These systems have been reported to show great performance, though not fully developed as they still lack experimental studies [3]. The study of Mokha et al. [7] on flat sliding bearings showed a good agreement between numerical and experimental results when experimentally derived parameters of μ_{max} = 0.12, μ_{min} = 0.0389, and α = 15.75 s/m under bearing pressure of 3.45 MPa were adopted. Also a study by Xu et al. [18] on static friction of curved sliders under low to moderate earthquakes showed that for isolators with low friction coefficients, an increase of breakaway-to-minimum ratio from 1 to 4 induced moderate changes in bearing shear forces, superstructure drift and floor accelerations, while for moderate and high isolators' friction the breakaway-to-minimum ratio of 2 introduced no significant changes.

Poornima and Babu [30] reported that for a 15 story RC building, FPS were the best in seismic isolation in comparison with Lead Rubber Bearings (LRB) and high damping rubber bearings. They concluded that FPS with damping ratio of 0.05 and friction coefficient from 0.03 to 0.06 could increase isolated building period by 37.97 % and top floor displacement by 29.05 %, while decreasing story acceleration, story shear and story drifts by 56.31 %, 63.828 % and 44.15 %, respectively. However, previous study on a 5 story RC building by Pokhrel et al. [31] had reported that both LRB and FPS can reduce base shear force, inter-story drifts and top floor acceleration by 50 %, and adding that while LRBs were the best in reducing elastic base shear as well as inter-story drifts, FPS showed greater control of isolator displacement for adopted bearing characteristics and wider hysteresis loop under far-fault earthquakes.

To date, there have been appreciable modifications of sliding bearings, and a substantial number of existing researches seem to have been mainly focusing on modified bearings (double, triple, and quintuple FPS), with less literature on the conventional (flat and single curved) bearings despite of their greater economic advantages [7, 9], and hence their potential applicability in developing countries. Furthermore, the existing literature on conventional sliding bearings seem to have been partially developed in terms of Full Structural Response Investigation (FSRI) on the behavior of both bearings and isolated superstructure when exposed to near and far-fault ground motions. Most importantly, studies that fully examine seismic isolation behavior in terms of FSRI (energy dissipation, top and base floor displacements, story drifts, superstructure accelerations, base shear force and accelerations, isolator's effective and post-yield stiffness variation, optimal control of bearing's hysteretic behavior, and control on the time instants for the occurrence of structural peak responses) under different types of earthquakes seem to have not yet been conducted. The authors of this study believe that in order to gain insights on effective performance of seismic isolation under different types of seismic loads, it is necessary to conduct studies that are pertinent to FSRI. In this regard, the main purpose of this study was to control the responses of a 10 story RC building model isolated by conventional sliding bearings and exposed to both near and far-fault earthquake ground motions, by applying FSRI to ensure a full seismic response control on the above building. In addition to the governing equations for flat and single-curved surface sliders, the study also attempted to formulate an improved equation for curved slider having its stiffness as a tenth of the first story structure and compared its results with ones from the existing curved slider equation.

2. Methods

In order to achieve the objectives of this study, equations governing the dynamic behavior of superstructure and substructure were first defined. Furthermore, a numerical study on seismic response control of a 10 story RC building model isolated by flat and curved surface sliding bearings was conducted by using the aforementioned equations.

2.1. Governing Equations

The equation governing a dynamic motion of any structure that is fixed at its base and exposed to a dynamic load can be written as:

$$M_{n \times n} \ddot{U}_{n \times 1} + C_{n \times n} \dot{U}_{n \times 1} + K_{n \times n} U_{n \times 1} = -M_{n \times n} R_{n \times 1} \left\{ \ddot{U}_g \right\}. \tag{1}$$

For a dynamic motion of a structure isolated at its base, the governing differential equations can be expressed as:

$$\begin{pmatrix} [I] & \left[\varnothing^T MR \right] \\ \left[R^T \varnothing \right] & \left[R^T MR + M_b \right] \end{pmatrix}_{(m+1)(m+1)} \left\{ \begin{matrix} \ddot{U}^* \\ \ddot{U}_b \end{matrix} \right\} + \begin{pmatrix} [2\xi_i \omega_i] & 0 \\ 0 & [C_b] \end{pmatrix}_{(m+1)(m+1)} +$$

$$+ \begin{pmatrix} \left[\omega_i^2 \right] & 0 \\ 0 & [K_b] \end{pmatrix}_{(m+1)(m+1)} \left\{ \begin{matrix} U^* \\ U_b \end{matrix} \right\}_{(m+1) \times 1} = - \begin{bmatrix} \varnothing^T MR \\ R^T MR + M_b \end{bmatrix}_{(m+1) \times 1} \ddot{U}_{g\,1 \times 1}, \tag{2}$$

Where $U_n = \phi_{n \times m} U_{m \times n}^*$ and ϕ is the modal matrix of fixed base superstructure normalized with respect to mass, and is used to find the diagonal matrices: $\varnothing^T M \varnothing = I,\ \varnothing^T K \varnothing = \omega^2,\ \varnothing^T C \varnothing = 2\xi \omega,$ where ω is diagonal matrix of natural frequencies of fixed base structure, ξ is diagonal matrix of damping ratio of fixed base structure, $U^*, \dot{U}^*, \ddot{U}^*$ are model displacement, velocity and acceleration vectors relative to the base, m is the number of eigenvectors retained in the analysis, ξ_i is modal damping ratio and ω_i is natural frequency of fixed base structure for mode i, M is the diagonal superstructure mass matrix, C is superstructure damping matrix, K is the superstructure stiffness matrix, R is influence matrix, M_b is diagonal mass matrix of rigid base, K_b is resultant stiffness matrix of elastic isolation elements, C_b is resultant damping matrix of viscous isolation element, $U_b,\ \dot{U}_b,\ \ddot{U}_b$ are vectors of base displacement, velocity and accelerations relative to the ground respectively, $\ddot{U}_g$ is vector of ground acceleration, f is vector containing forces mobilized in the nonlinear elements of the isolation system. Equation (2) has been adopted in 3D-BASIS Software by Tsopelas et al. [32]. However, for simplicity and easy solution by 4th order Runge-Kutta algorithm, this equation can also be expressed as shown below:

a) The equation governing a dynamic motion of superstructure can be written as:

$$M_{n \times n} \ddot{U}_{n \times 1} + C_{n \times n} \dot{U}_{n \times 1} + K_{n \times n} U_{n \times 1} = -M_{n \times n} R_{n \times 1} \left\{ \ddot{U}_g + \ddot{U}_b \right\}, \tag{3}$$

Where n is the number of floors, $M_{n \times n}$ is the diagonal superstructure mass matrix, $C_{n \times n},\ K_{n \times n}$ are the superstructure damping and stiffness matrices respectively, and $U_{n \times 1},\ \dot{U}_{n \times 1},\ \ddot{U}_{n \times 1}$ are vectors of superstructure displacement, velocity, and acceleration for n floors, respectively.

From equation (3), $\ddot{U}_{n \times 1}$ can be expressed as:

$$\ddot{U}_{n \times 1} = -\left(M_{n \times n} R_{n \times 1} \left(\ddot{U}_g + \ddot{U}_b \right) + C_{n \times n} \dot{U}_{n \times 1} + K_{n \times n} U_{n \times 1} \right) \Big/ M_{n \times n}. \tag{4}$$

Then, Equation (4) yields

$$\ddot{U}_{n \times 1} = -\left(\ddot{U}_g + \ddot{U}_b \right) - \left(C_{n \times n} \dot{U}_{n \times 1} + K_{n \times n} U_{n \times 1} \right) \Big/ M_{n \times n}. \tag{5}$$

b) The equation governing a unidirectional dynamic motion of base structure can be expressed as:

$$R_{1\times n}^{T} M_{n\times n} \left\{ \left\{ \ddot{U} \right\}_{n\times 1} + R_{n\times 1} \left\{ \ddot{U}_b + \ddot{U}_g \right\}_{1\times 1} \right\} + M_{b\,1\times 1} \left\{ \ddot{U}_b + \ddot{U}_g \right\}_{1\times 1} +$$
$$+ C_{b\,1\times 1} \left\{ \dot{U}_b \right\}_{1\times 1} + K_{b\,1\times 1} \left\{ U_b \right\}_{1\times 1} + \left\{ f \right\}_{1\times 1} = 0,$$

(6)

Where, $R_{1\times n}^{T}$ is the transpose of the influence matrix, 1×1 is the index representing a one by one matrix or simply a single value (for each time step) when unidirectional motion is considered.

Rearranging Equation (6),

$$R_{1\times n}^{T} M_{n\times n} \ddot{U}_{n\times 1} + R_{1\times n}^{T} M_{n\times n} R_{n\times 1} \left\{ \ddot{U}_b + \ddot{U}_g \right\}_{1\times 1} + M_{b\,1\times 1} \ddot{U}_{b\,1\times 1} +$$
$$+ M_{b\,1\times 1} \ddot{U}_{g\,1\times 1} + C_{b\,1\times 1} \dot{U}_{b\,1\times 1} + K_{b\,1\times 1} U_{b\,1\times 1} + f_{1\times 1} = 0.$$

(7a)

Equation (7a) can be rearranged such that $\ddot{U}_{b\,1\times 1}$ is easily obtained:

$$\ddot{U}_{b\,1\times 1} \frac{\left(R_{1\times n}^{T} M_{n\times n} R_{n\times 1} + M_{b\,1\times 1} \right)}{A_b} =$$

$$= \frac{-\left(R_{1\times n}^{T} M_{n\times n} \ddot{U}_{n\times 1} + R_{1\times n}^{T} M_{n\times n} R_{n\times 1} \ddot{U}_{g\,1\times 1} + M_{b\,1\times 1} \ddot{U}_{g\,1\times 1} + C_{b\,1\times 1} \dot{U}_{b\,1\times 1} + K_{b\,1\times 1} U_{b\,1\times 1} + f_{1\times 1} \right)}{B_b}.$$

(7b)

Then, the base floor acceleration for each time step can be solved as:

$$\ddot{U}_{b\,1\times 1} = A_b^{-1} * B_b.$$

(7c)

The superstructure mass, stiffness and damping matrices can be formulated as:

$$\left[M_{n\times n} \right] = \begin{bmatrix} m_1 & 0 & 0 & 0 & 0 & 0 \\ 0 & m_2 & 0 & 0 & 0 & 0 \\ 0 & 0 & m_3 & 0 & 0 & 0 \\ 0 & 0 & 0 & ... & 0 & 0 \\ 0 & 0 & 0 & 0 & ... & 0 \\ 0 & 0 & 0 & 0 & 0 & m_n \end{bmatrix},$$

(8)

$$\left[K_{n\times n} \right] = \begin{bmatrix} k_1 + k_2 & -k_2 & 0 & 0 & 0 & 0 \\ -k_2 & k_2 + k_3 & -k_3 & 0 & 0 & 0 \\ 0 & -k_3 & k_3 + k_4 & -k_3 & 0 & 0 \\ 0 & 0 & ... & ...+... & ... & 0 \\ 0 & 0 & 0 & ... & ...+... & -k_n \\ 0 & 0 & 0 & 0 & -k_n & k_n \end{bmatrix}.$$

(9)

In this study, the superstructure damping matrix $\left[C_{n\times n} \right]$ was calculated from $\left[M_{n\times n} \right]$ and $\left[K_{n\times n} \right]$ based on Rayleigh formula [4, 33], which is defined as shown in Equation (10).

$$\left[C_{n\times n} \right] = \alpha_0 \left[M_{n\times n} \right] + \alpha_1 \left[K_{n\times n} \right].$$

(10)

To obtain the coefficients α_0 and α_1, Equation (11) can be used [34].

$$\frac{1}{2}\begin{bmatrix} \dfrac{1}{w_i} & w_i \\[2mm] \dfrac{1}{w_j} & w_j \end{bmatrix}\begin{Bmatrix} \alpha_0 \\ \alpha_1 \end{Bmatrix} = \begin{Bmatrix} \xi_i \\ \xi_j \end{Bmatrix}, \tag{11}$$

where w_i, w_j and ξ_i, ξ_j are natural frequencies and damping ratios of the non-isolated structure with i^{th} and j^{th} modes respectively. The damping ratios at i^{th} and j^{th} can be assumed as shown in [4].

The hysteretic behavior of sliding bearings has been modelled by a substantial number of researchers using Bouc-Wen model for dynamic analysis of bilinear and non-linear hysteretic systems [6, 32].This model is adopted in this study for hysteretic force (f) of flat and curved bearings.

For flat surface sliding bearings:

$$f_x = \mu W Z_x. \tag{12}$$

For single curved surface sliding bearings:

$$f_x = \frac{w}{R_{eff}} U_b + \mu W Z_x. \tag{13}$$

Apart from Eq. (12) and (13), a new formulation typical to Eq. (13) is formulated as shown in Eq. (14) where the isolator stiffness is directly related to the first story stiffness through the value K_c. Eq. (12)–(14) are all adopted and compared to examine their effectiveness. Particularly, Eq. (14) is compared with the existing Eq. (13) to examine its possible applicability for other structures with same properties as one investigated in this study.

$$f_x = K_c U_b + \mu W Z_x. \tag{14}$$

Where:

$$\mu(\dot{u}) = \mu_{max} - (\mu_{max} - \mu_{min})e^{-\alpha|\dot{u}|}, \tag{15}$$

f_x is hysteretic force in x-direction, μ is the coefficient of friction, α is a constant and the parameters μ_{min} and μ_{max} describe the friction coefficients at essentially zero and high velocities, respectively, R_{eff} is the radius of curvature, W is the total weight of the structure calculated as: $W = \left(\sum_{i-1}^{10} mi + M_b\right) \times g$, where, g is the gravity acceleration and mi is the mass at the ith floor; K_c is the tenth of the first story stiffness, and Z_x is a hysteretic component of the unidirectional Wen's non-linear model and can be derived from Equation (16).

$$\dot{Z}_x = \left[A\dot{U}_{bx} - \dot{U}_{bx}Z_x^2\left(y\ sign(\dot{U}_{bx}Z_x) + \beta\right)\right]\Big/U_y, \tag{16}$$

where A, γ, β are dimensionless quantities, x stands for the base motion in x-direction, U_y is the yield displacement. The idealized hysteretic behavior of the aforementioned bearings is shown in Fig. 1.
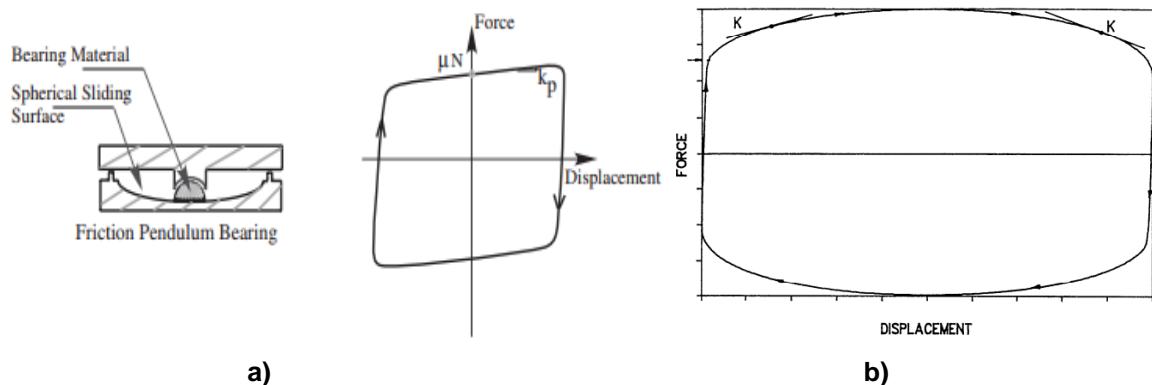

Figure 1. Idealized force-displacement relations: a) curved, b) flat surface sliding bearings.

Dushimimana, A., Singirankabo, E., Kathumbi, L.K.

In this study, Eq. (5) and (7c) derived from the general equations of superstructure and base motion respectively, and Eq. (12) through (16) were solved by 4th order Runge-Kutta algorithm in MATLAB environment. The detailed procedures involved in this algorithm can be found in [34].

2.2. Numerical Study

Responses of 10 story structure model under four input parameters and three earthquake ground motions were investigated with respect to flat and curved surface sliding bearings defined by Equations (12)–(14). The earthquakes were sourced from PEER strong ground motions [35], then filtered and corrected using Seismosignal Software(SS). The characteristics of these earthquakes are summarized in Table 1. It is important to mention that various kinds of excitations have been proposed to investigate dynamic behavior of isolated structures, such as the use of blasts [36] and micro tremors [37], however, this study focused on the use of near and far-fault earthquakes occurred in the past. The engineering data used for the above structure are shown in Table 2. Additionally, structural masses lumped at each floor, story height of 3 m for each floor and overall damping ratio of 5 percent are assumed for the investigated structure. The values of K_b, M_b and C_b are assumed equal to ones of the first story stiffness, mass and damping, respectively. K_c is taken as the tenth of the first story stiffness, for each input. Yield strength of the isolator is computed as $U_y = F_y / K_b$, and the friction parameters adopted are: μ_{min} = 0.02, μ_{max} = 0.15, R_{eff} = 0.435 m, A =1, β = 0.1, and γ = 0.9. It is important to note that these friction parameters and data shown in Table 2 for Input 2 have been previously adopted in [23]. The response quantities of interest investigated are: Energy Dissipation Capacity (EDC), Maximum Isolator Displacement (MID), Maximum Isolator Force (MIF), top floor displacements, story drifts, base floor shear force and accelerations, isolator's effective and post-yield stiffness variation, peak story accelerations, peak story shear forces, optimal control of bearing's hysteretic behavior (by checking the relationship among MID, MIF and EDC), and control on the Time Instants (TIs) for the occurrence of structural peak story displacements under the aforementioned earthquakes.

Table 1. Characteristics of used earthquakes.

Earthquake	Component	PGA (m/s²)	PGV(m/s)	PGD(m)	Te(s)	Type	Duration (s)
Elcentro	NS	3.42	0.32	0.09	2.88	LP	56.52
Düzce	EW	8.05	0.63	0.12	0.96	NF	55.85
Kobe	NS	8.03	0.92	0.18	1.10	NF	49.93

PGA, PGV, and PGD are peak ground acceleration, velocity and displacement respectively, Te: predominant period, NF: Near Fault, LP: Long period, NS: North-South direction, EW: East-West direction

Table 2. Input parameters.

		Story 1	Story 2	Story 3	Story 4	Story 5	Story 6	Story 7	Story 8	Story 9	Story 10
Input 1	m	400000	520000	520000	520000	520000	520000	520000	520000	520000	520000
	k	2187e5	800e5	800e5	800e5	800e5	800e5	800e5	800e5	800e5	800e5
Input 2	m	8385063	8285063	8285063	8285063	8285063	8285063	8285063	8285063	8285063	8285063
	k	10.75e9	8.78e9	6.80e9	5.65e9	4.90e9	4.38e9	4.01e9	3.12e9	3.50e9	3.33e9
Input 3	m	8385063	8285063	8285063	8285063	8285063	8285063	8285063	8285063	8285063	8285063
	k	10.75e11	8.78e11	6.80e11	5.65e11	4.90e11	4.38e11	4.01e11	3.12e11	3.50e11	3.33e11
Input 4	m	8385063	8285063	8285063	8285063	8285063	8285063	8285063	8285063	8285063	8285063
	k	10.75e12	8.78e12	6.80e12	5.65e12	4.90e12	4.38e12	4.01e12	3.12e12	3.50e12	3.33e12

Abbreviations: m: mass of superstructure (in Kg), k: stiffness of superstructure in (in N/m)

Insights on the inputs shown in Table 2 demonstrate that both mass and stiffness values are kept equal under Input 1 for all floors except for 1st story floor. On the other hand, Input 2 has the same story mass but varied story stiffness. Furthermore, Input 3 and 4 are of similar trend as Input 2 except that their story stiffness are 10^2 and 10^3 times the story stiffness of Input 2, respectively. Existing literature demonstrates that superstructure stiffness can be increased through retrofitting and strengthening [38–40], use of shear walls and braced frames [41, 42], as well as central core, tube and double tube systems. That is, increasing superstructure stiffness is important because the current building industry is toward larger floors, longer spans and taller buildings, all of which may require sufficient structural stiffness against both axial and dynamic loads. In this regard, the story stiffness was increased to examine the effect of superstructure stiffening on behavior of the used bearings.

3. Results and Discussion

3.1. Top Floor Displacements

Floor displacement control is vital, as very large and dangerous superstructure displacements can occur in earthquake-prone areas [43], hence damaging sensitive equipment in buildings, especially those located in NF zones where long period earthquakes can occur [44]. Under moderate earthquakes like Elcentro, the top floor relative displacements $\left(U_{top}\right)$ are observed to be equal for all equations under each input as can be seen in Fig. 2. That is, $\left(U_{top}\right)$ are observed to be approximately 0.28, 0.13, 0.0041 and 0.00044 m for Inputs 1, 2, 3 and 4 respectively.
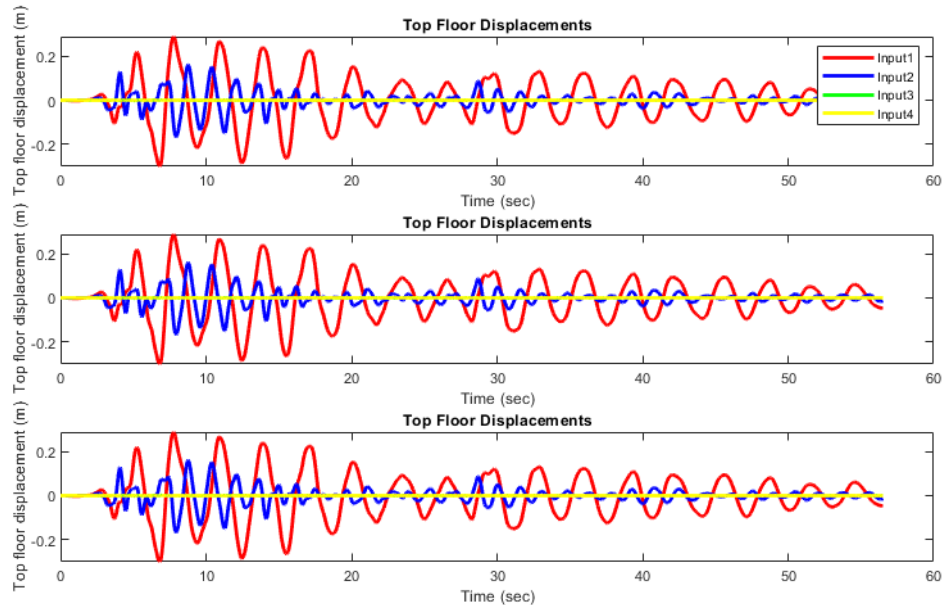

Figure 2. Top floor displacements under equations (12) to (14) (from top to bottom) – Elcentro.

Similar trends are also observed for Kobe earthquake, where $\left(U_{top}\right)$ of approximately 0.4, 0.5, 0.0075, and 5.78e^{-4} m are obtained for Input 1, 2, 3 and 4, respectively under Equations (12)–(14). Based on this observation, Input 1 is the most favourable as it results in reasonably reduced $\left(U_{top}\right)$ for a 10 story structural model compared to other inputs. This shows the importance of using equal stiffness for all floors in reduction of $\left(U_{top}\right)$ under strong earthquake by approximately 10 %.

Like Elcentro and Kobe earthquake, Duzce is also observed to result in similar trend of $\left(U_{top}\right)$ with approximately 0.2, 0.2, 0.0073, and 6.0279e^{-4} m for Input 1, 2, 3 and 4, respectively. However, using similar story stiffness values under Duzce and Elcentro result in unwanted long-lasting $\left(U_{top}\right)$ peaks over nearly the entire duration of each earthquake (Fig. 2, 4), which can cause substantial cracks in structural components of the superstructure. Deep insights on this unwanted behavior can be found referring to Table 4, where the time instants of the occurrence of maximum story peaks are observed to alter significantly between story 5 to 6 and 9 to 10 under Duzce and 7 to 8 and 8 to 9 under Elcentro, and hence outlining that use of similar superstructure stiffness may be unreliable in controlling superstructure displacements when such earthquakes occur. Furthermore, the pronounced long-lasting $\left(U_{top}\right)$ peaks over the entire duration of Elcentro and Duzce lead to suggesting that PGA alone may not characterize the earthquake severity, since those two earthquakes have significantly different PGA values as can be seen in Table 1.
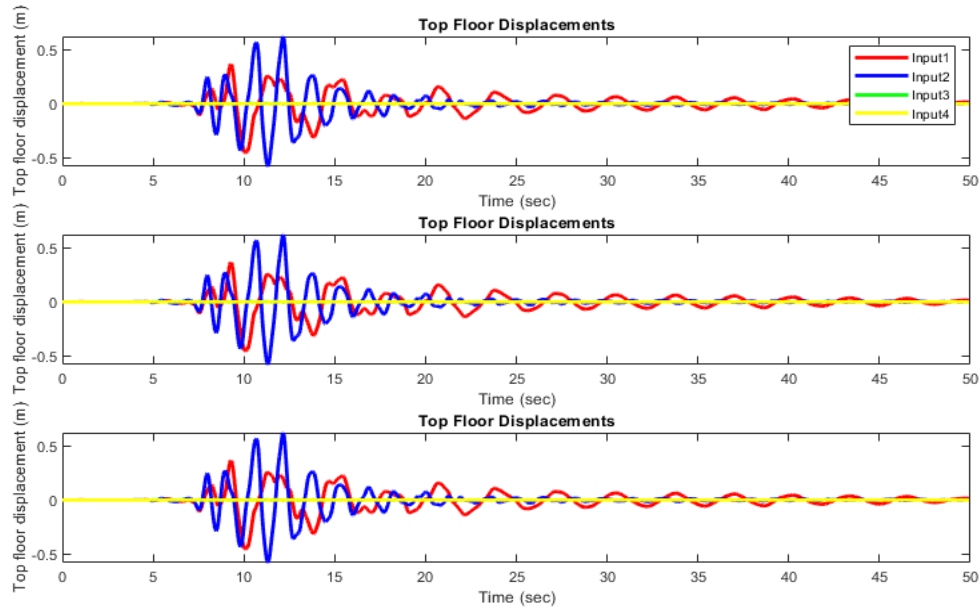
Figure 3. Top floor displacements under equations (12) to (14) (from top to bottom) – Kobe.
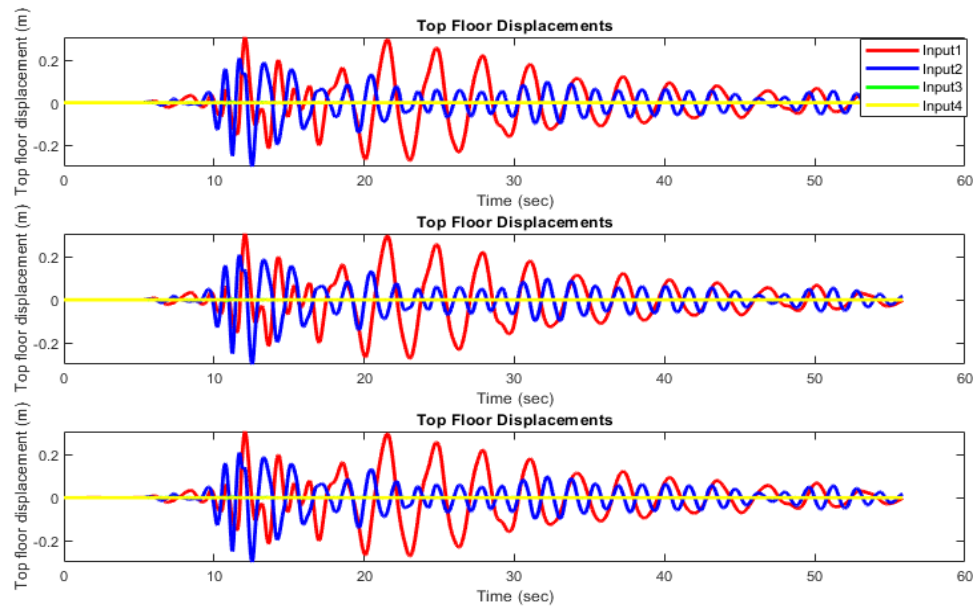

Figure 4. Top floor displacements under equations (12) to (14) (from top to bottom) – Duzce.

From the above results, it can be noted that Equations (12)–(14) perform similarly and equally in reducing top floor displacement $\left(U_{top}\right)$ for each used input. Besides, under all three earthquakes it is seen that the resulting $\left(U_{top}\right)$ are smaller when moderate LP earthquakes like Elcentro are used, rather than strong NF ones like Kobe. However, though Duzce is also classified as a strong NF earthquake, this earthquake and Elcentro are observed to result in comparable $\left(U_{top}\right)$ as can be seen in Fig. 2 and 4. This may be interpreted as Duzce having a single PGA at around 10 s, followed by a sharp decrease in PGA and thereafter levelling off all along until its final duration time, a nature that is far different from Kobe's which has successive peak fluctuations over 8-13 s interval of time. Additionally, this shows that some NF earthquakes may behave like LP moderate ones, regardless of their PGA.

Under all earthquakes, the increase in stiffness leads to decrease in $\left(U_{top}\right)$, and all the earthquakes tend to result in approximately similar displacement profiles as stiffness becomes large, which indicate that $\left(U_{top}\right)$ of very stiff superstructure may not significantly be affected by the magnitude of the earthquake. Further observation shows that LP moderate & NF with smaller PGV earthquakes tend to cause the structure with varied story stiffness perform better than the structure with

constant story stiffness in terms of $\left(U_{top}\right)$ reduction, contrary to NF with higher PGV earthquakes where the effect is less pronounced. Looking at the resulting maximum $\left(U_{top}\right)$, it can be seen that Equation (12) results in the smallest $\left(U_{top}\right)$ under all earthquakes for Inputs 1 and 2, thus making flat slider the most effective in terms of $\left(U_{top}\right)$ reduction for less stiffened superstructure.

Table 3. Structural responses under all inputs and all earthquakes.

EARTHQUAKE		KOBE			DUZCE			ELCENTRO		
SLIDER		Eq.(12)	Eq.(13)	Eq.(14)	Eq.(12)	Eq.(13)	Eq.(14)	Eq.(12)	Eq.(13)	Eq.(14)
Input1	$\ddot{U}_{b\max}$	3.6113	3.2088	3.5292	3.6556	2.7416	3.09	1.0847	0.9479	0.9804
	U_{top}	0.3746	0.403	0.3792	0.209	0.2682	0.235	0.2743	0.2825	0.2771
	$F_{sb\max}$	1.44e06	1.28e6	1.41e6	1.45e6	1.10e6	1.24e6	4.34e5	3.79e5	3.92e5
Input2	$\ddot{U}_{b\max}$	11.8702	9.3349	15.5153	8.1562	6.3273	7.5064	5.8244	3.9769	5.0927
	U_{top}	0.4881	0.5276	0.5067	0.2227	0.2443	0.2382	0.1224	0.1386	0.1288
	$F_{sb\max}$	9.26e7	7.83e7	9.05e7	6.76e7	5.31e7	6.29e7	4.56e7	3.33e7	4.13e7
Input3	$\ddot{U}_{b\max}$	0.9279	0.9252	1.3921	4.067	4.0562	3.4225	2.4584	2.448	1.9813
	U_{top}	0.0075	0.0075	0.0076	0.0073	0.0073	0.0075	0.0041	0.0041	0.0041
	$F_{sb\max}$	7.63e6	7.63e6	7.22e6	3.20e7	3.19e7	2.62e7	1.99e7	1.99e7	1.58e7
Input4	$\ddot{U}_{b\max}$	0.1731	0.1728	0.1701	0.7988	0.7974	0.6317	0.8018	0.8031	0.7074
	U_{top}	5.78e-4	5.78e-4	5.84e-4	6.03e-4	6.03e-4	6.08e-4	4.38e-4	4.36e-4	4.4e-4
	$F_{sb\max}$	1.45e6	1.45e6	1.42e6	6.70e6	6.69e6	5.30e6	5.78e6	5.79e6	5.57e6

Abbreviations: $\ddot{U}_{b\max}$ is base floor acceleration, U_{top} is top floor displacement, $F_{sb\max}$ is base shear force.

3.2. Base Floor Accelerations and Base Shear Forces

Looking at the resulting maximum base shear forces $\left(F_{sb\max}\right)$ in Table 3, it can be seen that for very high stiffness all the used equations result in approximately equal $F_{sb\max}$ values of $1.9e^7$ and $5.7e^6$ N for Elcentro, $7.6e^6$ and $1.4e^6$ N for Kobe, $3.2e^7$ and $6.677e^6$ N for Duzce under Inputs 3 and 4, respectively. Similarly, approximately equal $\ddot{U}_{b\max}$ values of 2 and 0.8 m/s² for Elcentro, 1 and 0.2 m/s² for Kobe, 4 and 0.7 m/s² for Duzce are observed under the respective inputs. On the other hand, it can be seen that for all the used equations, the smaller the base acceleration the smaller the shear force, as expected [45]. Focusing on moderate stiffness, Input 1 is observed to result in smaller $F_{sb\max}$ than that from Input 4 for all the equations and earthquakes. Besides, Input 2 results in the highest value of $F_{sb\max}$ for all used equations and earthquakes, whereas Input 1 results in the least. This reveals that Input 1 can be the most effective in terms of $F_{sb\max}$ reduction compared to other inputs. Additionally, it can be seen that Equation (13) results in the smallest base shear force for Input 1 and 2, whereas Equation (14) results in the smallest force in all other inputs and earthquakes.

Focusing on the resulting maximum base accelerations $\left(\ddot{U}_{b\max}\right)$ in Table 3 and Fig. 5, it can be seen that all equations perform equally in reducing or increasing accelerations for each input. It is clear that all equations result in $\ddot{U}_{b\max}$ of approximately 1, 2 and 0.8 m/s² for Inputs 1, 3, and 4 respectively, except for Input 2 where Equation (13) reduces $\ddot{U}_{b\max}$ more than the other equations.
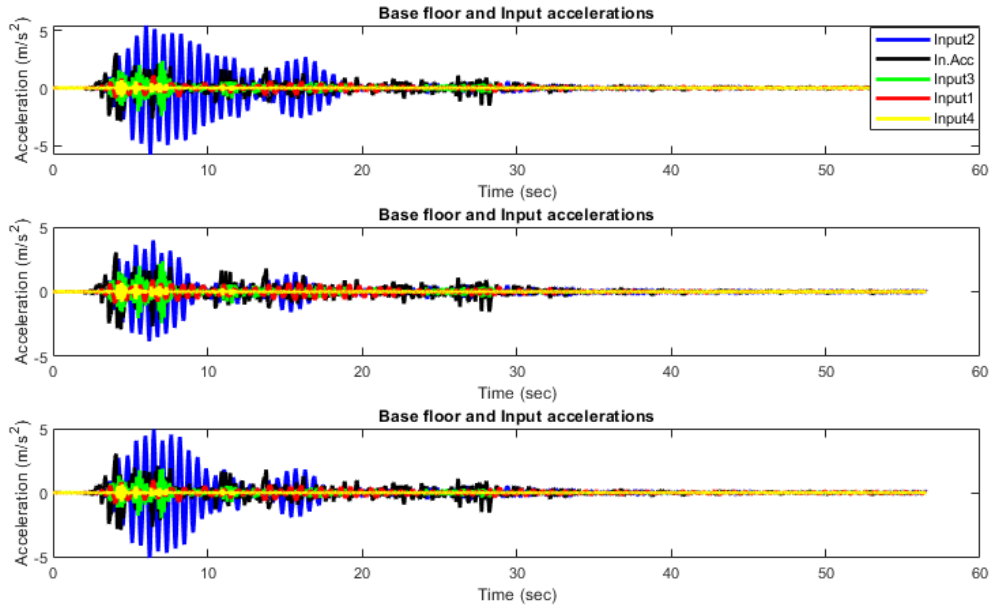
**Figure 5. Base floor & Input accelerations under equations
(12) to (14) (top to bottom) –Elcentro.**

On the other hand, Input 1 results in slightly smaller $F_{sb\,\max}$ than that of Input 4 for all equations, and when Input 1 and 3 are used, Equation (13) tends to result in the smallest $F_{sb\,\max}$ compared to both Equation (12) and (14) as seen in Table 3. This indicates that Equation (13) can be more effective for structures with moderate stiffness than Equation (12) under NF earthquake ground motions. Further observation from Fig. 5 and 6 shows that Input 2 amplifies $\ddot{U}_{b\,\max}$ under both Kobe and Elcentro earthquakes while keeping $\ddot{U}_{b\,\max}$ from Duzce approximately equal to Duzce acceleration, except for Equation (12) where a slight amplification of nearly 0.1 m/s² is observed as can be seen in Table 3 and Fig. 7. Contrarily to Input 2, Input 1 is observed to result in the most desirable $\ddot{U}_{b\,\max}$ values of approximately 3.6113, 3.2088 and 3.5292 m/s²; 3.6556, 2.7416, and 3.09 m/s²; 1.0847, 0.9479 and 0.9804 m/s² from Equations (12), (13), and (14) under Kobe, Duzce and Elcentro earthquakes, respectively. This makes Input 2 less viable in terms of $\ddot{U}_{b\,\max}$ reduction, though was proven to perform better than Input 1 in terms of superstructure story displacements control.
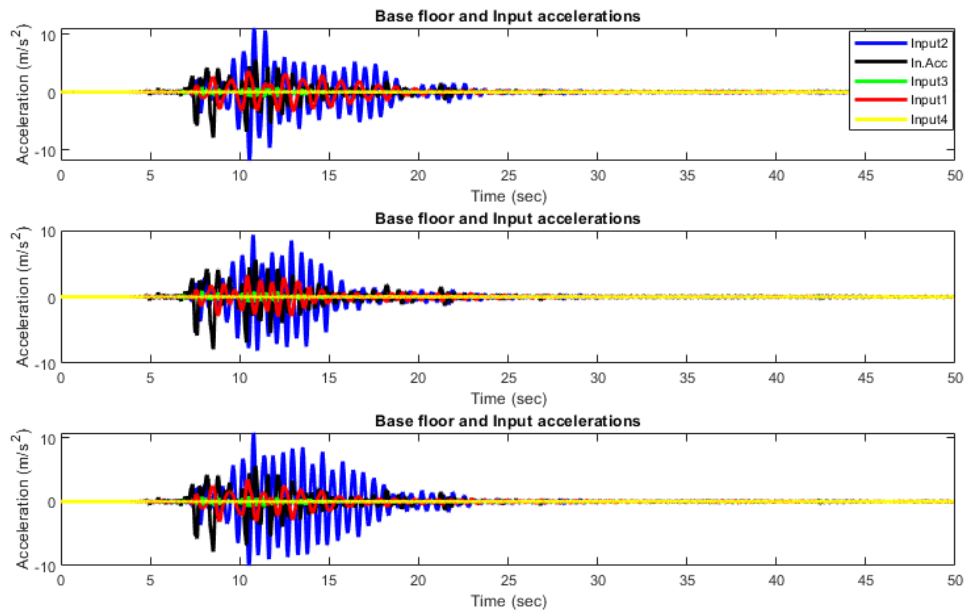

Figure 6. Base floor & Input accelerations for equations (12) to (14) (top to bottom) – Kobe.
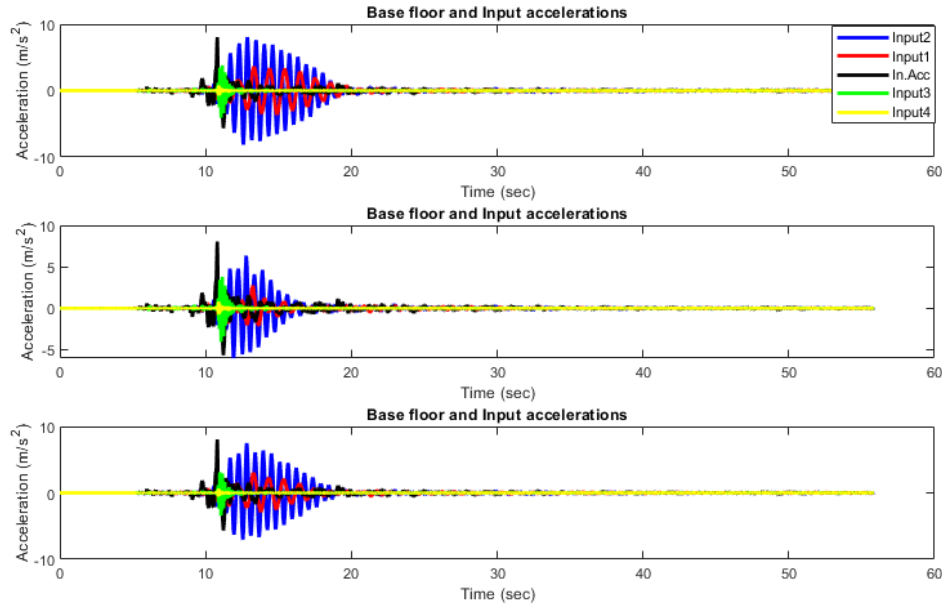
Figure 7. Base floor & Input accelerations for equations (12) to (14) (top to bottom) – Duzce.

On the other hand, a drastic increase in stiffness of the superstructure leads to drastic decrease in relative $\ddot{U}_{b\,\max}$ up to a value smaller than 1 m/s² as seen under Input 3 and 4 in Table 3. However, increasing stiffness can hinder reasonable isolator displacement as shown in Fig. 5, 6, 7, and Table 3. This is also confirmed by observing a substantial reduction of EDC, despite of the resulting reduced accelerations, hence indicating that stiffer systems can perform well in reducing the relative base shear forces and accelerations but poorly in dissipating sufficient energy as it will be shown in section 3.4. Overall, Input 1 and 3 can result in more benefits when considering shear forces, energy dissipation and base acceleration, but the former input can lead to large displacements for some earthquakes as explained in the previous section 3.1.

In order to make the isolator perform effectively by reducing $\ddot{U}_{b\,\max}$ and dissipating sufficient energy, Input 1 can be adopted for all investigated equations over other inputs. By prioritizing Input 1, it is clear from Table 3 that Equation (13) results in the smallest $\ddot{U}_{b\,\max}$ of approximately 3.2088, 2.7416, 0.9479 m/s² under Kobe, Duzce, and Elcentro, respectively, as compared to Equations (12) and (14) which result in 3.6113 and 3.5292 m/s², 3.6556 and 3.09 m/s², and 1.0847 and 0.9804 m/s², under the same respective earthquakes, thus making Equation (13) the most effective for the investigated structure. For example, deep insights under Duzce earthquake show that approximately 55.8, 65.5 and 61.6 % $\ddot{U}_{b\,\max}$ reduction are observed from Equation (12), (13), and (14), respectively, making Equation (13) the most effective.

3.3. Time Instant for the occurrence of story floor displacements

The Time Instants (TIs) for which the maximum floor displacements take place are examined and the observed values are shown in Table 4. Investigating the TIs for which the peak responses take place can provide insights on the rigid body motion behavior of the superstructure. For instance, authors in [20] observed that under Elcentro earthquake, a six story building isolated by FPS resulted in a TI of 4.51 s for the superstructure displacements. In this study, under NF earthquakes like Kobe with Inputs 1 and 4, the maximum displacements from all used equations are observed to simultaneously occur at nearly 10 and 8.5 s, respectively. Besides, the displacements under Inputs 2 and 3 are observed to result in negligible differences of approximately 1 s in the first four floors and 2 s in the last three floors, respectively. Under Elcentro, Input 2 results in TIs of approximately 8 s. Similarly, Inputs 3 and 4 result in TIs of approximately 3.66 and 4.4 s. However, Input 1 tend to alter TIs significantly with a difference of 6s longer for 8th floor compared to other floors, thus showing lack of rigid motion behavior and making this input ineffective for the studied 10 story building when moderate LP earthquake occurs. Similar trends when Input 1 is adopted are observed even when strong earthquake like Duzce (NF, but with smaller PGV than Kobe's) is used with a substantial difference in TI between the first and last five floors, whereas the remaining Inputs 2, 3, and 4 cause the TIs to happen at reasonable values for all floors of nearly 12, 11, and 11 s respectively. Overall, the type of earthquake ground motion and input parameter are observed to influence the TIs, and therefore, for full control of structural responses under dynamic loads, TIs should be investigated.

Table 4. Time Instants for the occurrence of story floor displacements.

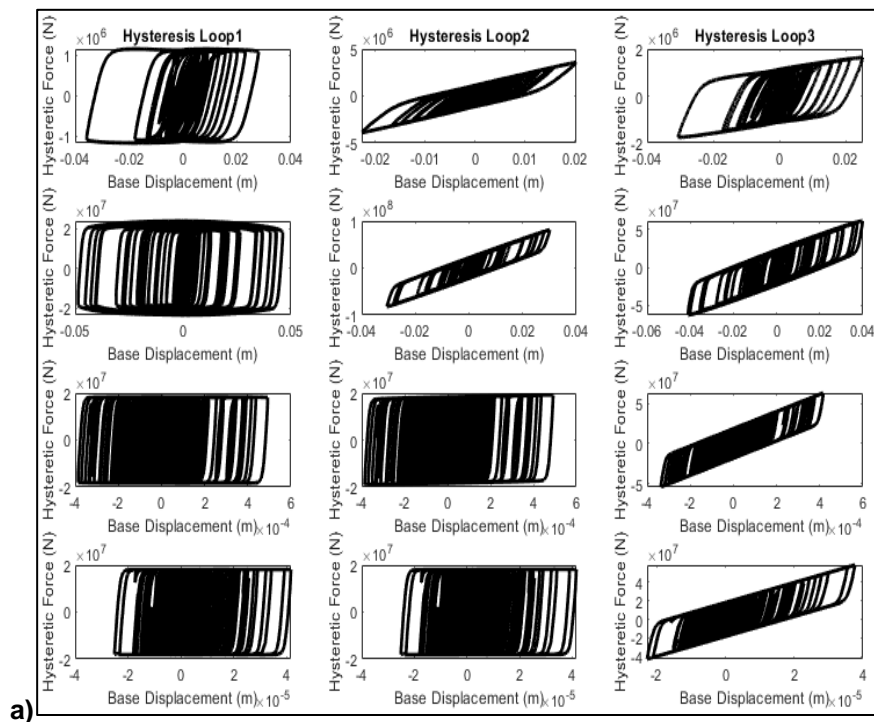| Earthquake		KOBE			DUZCE			ELCENTRO		
Slider	ST	Eq.(12)	Eq.(13)	Eq.(14)	Eq.(12)	Eq.(13)	Eq.(14)	Eq.(12)	Eq.(13)	Eq.(14)
Input 1	ST1	10.3	10.3	10.3	12.6	12.6	12.6	6.3	6.3	6.3
	ST2	10.3	10.3	10.3	13.1	13.1	13.1	6.4	6.4	6.4
	ST3	10.3	10.3	10.3	13.2	13.2	13.2	6.4	6.4	6.5
	ST4	10.3	10.3	10.3	13.2	13.2	13.2	6.5	6.5	6.5
	ST5	10.4	10.4	10.4	13.2	13.2	13.2	6.5	6.5	6.5
	ST6	10.3	10.3	10.3	21.4	21.4	21.4	6.5	6.5	6.5
	ST7	10.3	10.3	10.3	21.4	21.4	21.4	6.5	6.5	6.5
	ST8	10.2	10.2	10.2	21.5	21.5	21.5	12.5	12.5	12.5
	ST9	10.1	10.1	10.1	21.5	21.5	21.5	6.8	6.8	6.8
	ST10	10.1	10.1	10.1	12.1	12.1	12.1	6.8	6.8	6.8
Input 2	ST1	10.5	10.5	10.5	11.8	11.8	11.8	8.1	8.1	8.1
	ST2	10.5	10.5	10.5	11.8	11.8	11.8	8.1	8.1	8.1
	ST3	10.5	10.5	10.5	11.8	11.8	11.8	8.1	8.1	8.1
	ST4	10.5	10.5	10.5	11.9	11.9	11.9	8.1	8.1	8.1
	ST5	12.1	12.1	12.1	11.9	11.9	11.9	8.1	8.1	8.1
	ST6	12.1	12.1	12.1	11.9	11.9	11.9	8.1	8.1	8.1
	ST7	12.1	12.1	12.1	12.5	12.5	12.5	8.0	8.0	8.0
	ST8	12.1	12.1	12.1	12.5	12.5	12.5	8.0	8.0	8.0
	ST9	12.1	12.1	12.1	12.5	12.5	12.5	8.0	8.0	8.0
	ST10	12.2	12.2	12.2	12.5	12.5	12.5	7.9	7.9	7.9
Input 3	ST1	8.5	8.5	8.5	10.8	10.8	10.8	3.7	3.7	3.7
	ST2	8.5	8.5	8.5	10.8	10.8	10.8	3.7	3.7	3.7
	ST3	8.5	8.5	8.5	10.8	10.8	10.8	3.7	3.7	3.7
	ST4	8.5	8.5	8.5	10.8	10.8	10.8	3.7	3.7	3.7
	ST5	8.5	8.5	8.5	10.8	10.8	10.8	3.7	3.7	3.7
	ST6	8.6	8.6	8.6	10.8	10.8	10.8	3.7	3.7	3.7
	ST7	8.6	8.6	8.6	10.8	10.8	10.8	3.7	3.7	3.7
	ST8	10.5	10.5	10.5	10.8	10.8	10.8	3.7	3.7	3.7
	ST9	10.5	10.5	10.5	10.8	10.8	10.8	3.7	3.7	3.7
	ST10	10.5	10.5	10.5	10.8	10.8	10.8	3.7	3.7	3.7
Input 4	ST1	8.5	8.5	8.5	10.8	10.8	10.8	4.4	4.4	4.4
	ST2	8.5	8.5	8.5	10.8	10.8	10.8	4.4	4.4	4.4
	ST3	8.5	8.5	8.5	10.8	10.8	10.8	4.4	4.4	4.4
	ST4	8.5	8.5	8.5	10.8	10.8	10.8	4.4	4.4	4.4
	ST5	8.5	8.5	8.5	10.8	10.8	10.8	4.4	4.4	4.4
	ST6	8.5	8.5	8.5	10.8	10.8	10.8	4.4	4.4	4.4
	ST7	8.5	8.5	8.5	10.8	10.8	10.8	4.4	4.4	4.4
	ST8	8.5	8.5	8.5	10.8	10.8	10.8	4.4	4.4	4.4
	ST9	8.5	8.5	8.5	10.8	10.8	10.8	4.4	4.4	4.4
	ST10	8.5	8.5	8.5	10.8	10.8	10.8	4.4	4.4	4.4

3.4. Force-Displacement Relationship of Flat and Curved Sliding Bearings (EDC, MID, & MIF)

Control on the hysteretic loop shape and size and parameters of the isolator is vital as it has been reported that these mainly affect the responses of base-isolated structure [46]. Looking at Elcentro, EDCs from all equations vary significantly for Inputs 1 and 2. For instance, EDCs resulting under Input 2 from Equation (12), (13) and (14) are $5.13e^7$, $2.30e^7$ and $3.61e^7$J, respectively. Furthermore, under the same inputs and equations, maximum isolator force (MIF) are approximately $2.39e^7$, $8.08e^7$, and $6.13e^7$ N respectively. From this observation and considering the fact that high EDC

with small MIF leads to effective performance of the bearing [47], it is clear that flat slider defined by Equation (12) has the highest performance followed by Equation (14) and lastly the Equation (13). On the other hand, owing to very high superstructure stiffness from Inputs 3 and 4, approximately similar behavior is observed for Equations (12) & (13), except for Equation (14) which results in smaller EDC and higher MIF, performing seemingly poor as compared to other equations.

Focusing on the combined hysteresis loops from Inputs 1 and 2 in Fig. 8b, 9b, 10b, it can be observed that smaller superstructure stiffness used for Input 1 causes the isolator to similarly result in smaller isolator stiffness, whereas larger superstructure stiffness from Input 2 similarly results in larger isolator stiffness. That is, the more the superstructure stiffness is the more the isolator stiffness. This observation is used to compare the behavior of Equations (13) and (14) defined for curved surface slider, and in order to have deep insights, Inputs 2, 3, and 4 are shown in the same Figure. Referring to the above stiffness variation trend under Inputs 1 and 2, it can be observed from Inputs 2, 3, and 4 that Equation (13) tends to deviate from the expected behavior (i.e. the more the superstructure stiffness the more the isolator stiffness) by resulting in hysteresis with almost similar isolator stiffness as one of Equation (12). However, the reality is that Equation (13) was expected to continue increasing isolator stiffness as superstructure stiffness increases but it is observed to underestimate isolator stiffness for higher superstructure stiffness from Inputs 3 & 4, whereas Equation (14) keeps its conservative behavior, hence rendering the latter equation more effective. In this way, priority is given to Equation (14) rather than Equation (13) in the rest of discussions related to stiffened superstructure (Inputs 3 & 4).

Looking at EDC from Table 5 and Fig. 8 for Elcentro earthquake, Input 2 results in the highest EDC and MIF followed by Input 3. Similar to Elcentro, EDCs under Kobe from all sliders governed by Equations (12), (13) and (14) are observed to vary significantly based on both the slider and input type. For instance, under Input 2 EDCs of $7.84e^7$, $5.84e^7$, and $8.72e^7$ J are observed from Equations (12), (13) and (14), respectively as shown in Table 5 and Fig. 9. This indicates that the proposed Equation (14) can result in more energy dissipation than other equations, thus rendering it more effective than the existing curved slider formula denoted by Equation (13). However, similarly to Elcentro, for structures requiring high story stiffness (represented by Inputs 3 and 4), the proposed formula can perform better than the existing equation as can be seen in Fig. 9. Furthermore, under Input 2 the MIFs are observed to be $2.98e^7$, $2.14e^8$, and $1.42e^8$ N for Equations (12), (13) and (14), respectively. This indicates that flat slider can perform better in reducing MIF. A comparative perspective on both EDC and MIF demonstrates that flat surface slider can be the most effective for the studied building in terms of EDC and earthquake force reduction during NF Kobe earthquake. Considering other inputs, it is seen that for all equations, Input 2 results in the highest EDC followed by Inputs 1, 3 and 4, respectively. Duzce earthquake is, furthermore, observed to have similar trends as the ones from the previously investigated Kobe and Elcentro earthquakes (see Table 5 and Fig. 10).
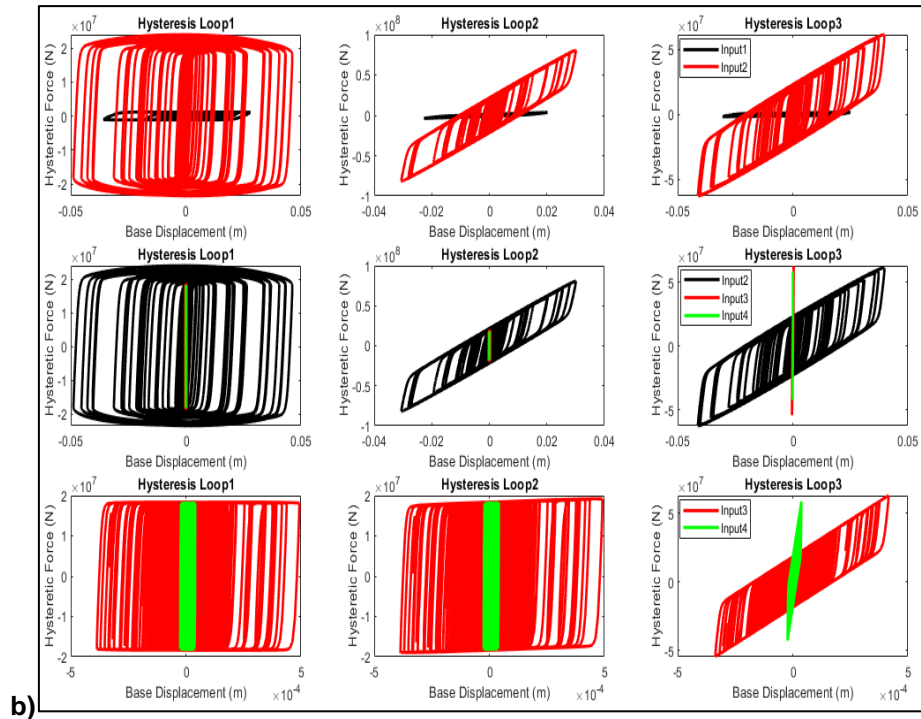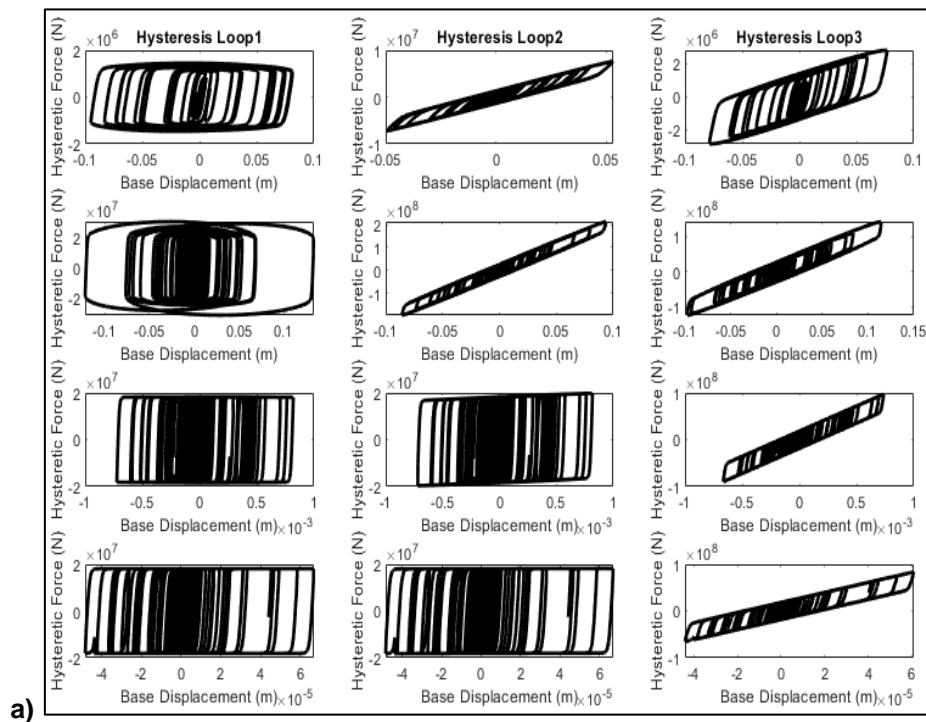
Figure 8. Force-displacement relations under Elcentro: a) Inputs 1 to 4 (top to bottom), and Hysteresis Loop1 to 3 (Equations (12) to (14)) for both a) and b).
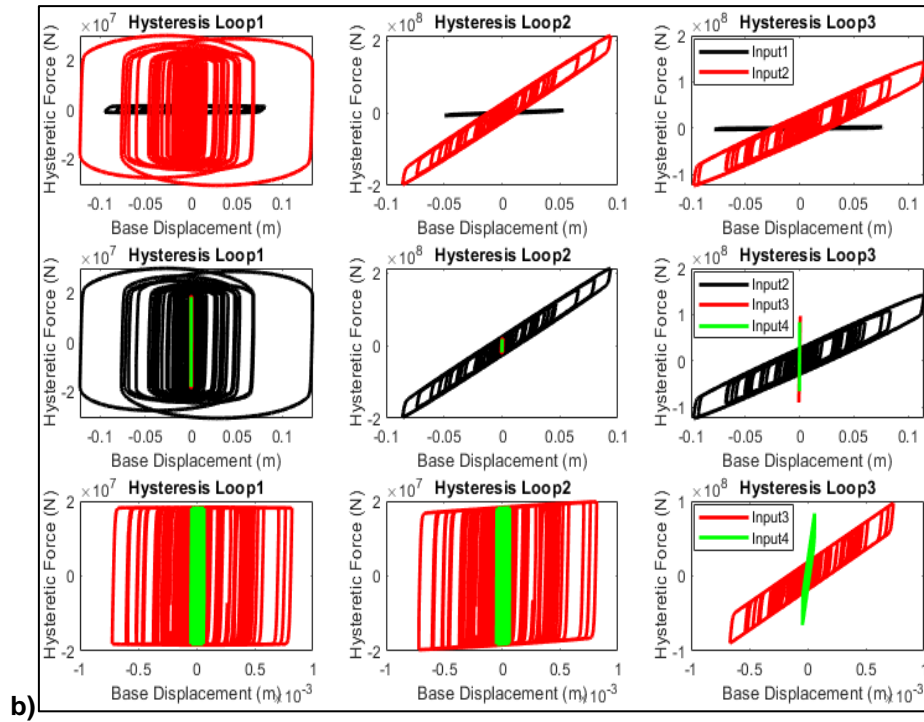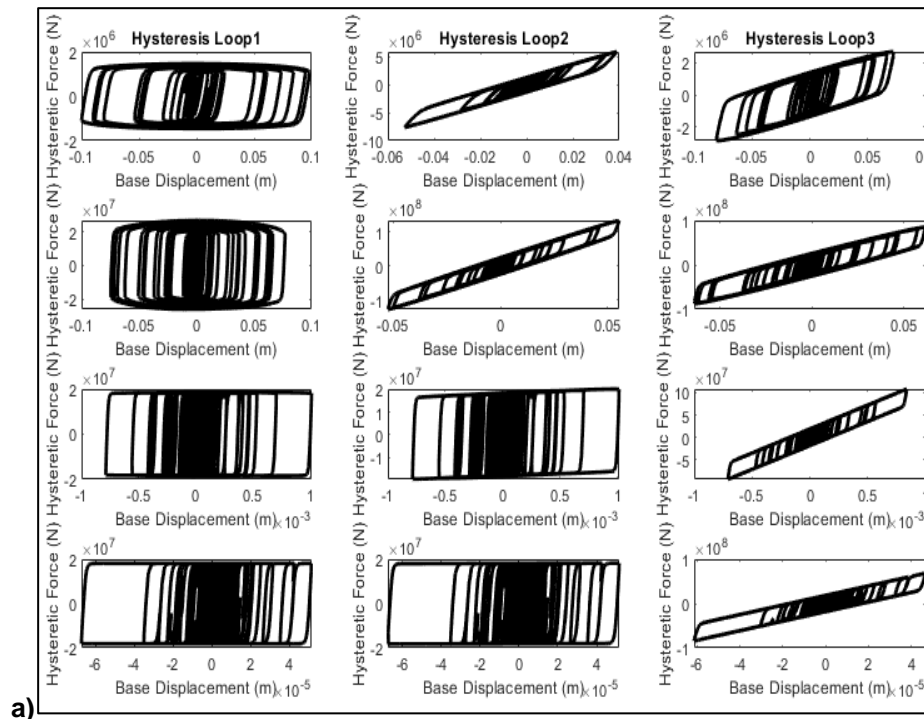
Figure 9. Force-displacement relations under Kobe: a) Inputs 1 to 4 (top to bottom), and Hysteresis Loop1 to 3 (Equations (12) to (14)) for both a) and b).

However, it is important to note that for all earthquakes, Equation (14) resulted in higher EDC than Equation (13) for Input1 and 2, and approximately similar EDC for Input 3 and 4, indicating that under the former inputs Equation (14) overestimates EDC as can been seen in Table 5. From this observation, the proposed formula can be reliable only when the increase in superstructure stiffness is expected. On the other hand, Equation (12) is observed to result in higher EDC than Equation (13) for Input 1 and 2, and nearly equal EDC for Input 3 and 4, indicating that under the former inputs, flat surface slider defined by Equation (12) can have better performance than curved one. Furthermore, a comparative perspective on EDC and MIF indicates that Input 1 and 2 can perform better as these inputs are capable of keeping both EDCs and MIF in a comparable range, while EDC and MIF from Inputs 3 and 4 are observed to differ significantly as seen in Fig. 8, 9, 10 and Table 5.
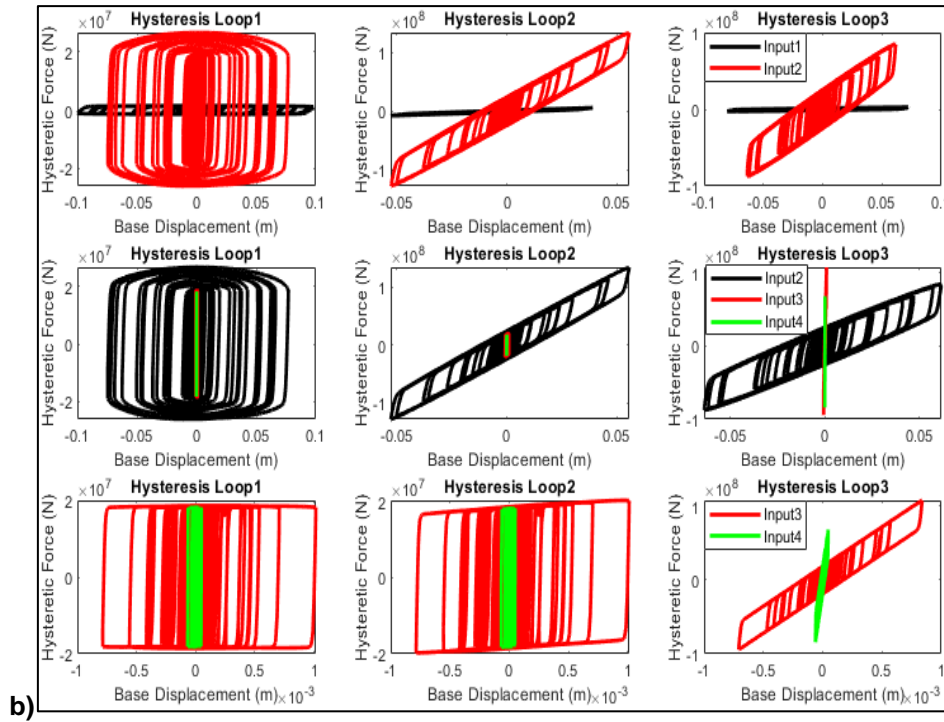
Figure 10. Force-displacement relations under Duzce: a) Inputs 1 to 4 (top to bottom), and Hysteresis Loop1 to 3 (Equations (12) to (14)) for both a) and b).

Further observations demonstrate that Equations (12) and (14) result in conservative hysteresis loop shapes from all inputs and earthquakes even when the story stiffness is increased up to e11 and e12, contrarily to curved surface slider defined by Equation (13), which tends to lose its stiffness trend as superstructure stiffness increases as can be seen Fig. 8b, 9b, 10b. In fact, curved slider from Equation (13) is observed to almost act as flat slider as the superstructure stiffness becomes large under Inputs 3 and 4. Similar observations are also made when NF earthquakes with high PGA like Kobe and Duzce are used, thus demonstrating that the conservative behavior of Equations (14) remains true under different types of earthquakes. Overall, for all earthquakes, flat slider is observed to be the most effective in both EDC and MIF reduction under all input parameters, followed by curved slider defined by Equation (14) under Inputs 3 and 4 or the curved slider defined Equation (13) under Input 1 and 2 in both EDC and MIF reduction.

Table 5. Energy Dissipation Capacity, Maximum Isolator Force and Displacement.

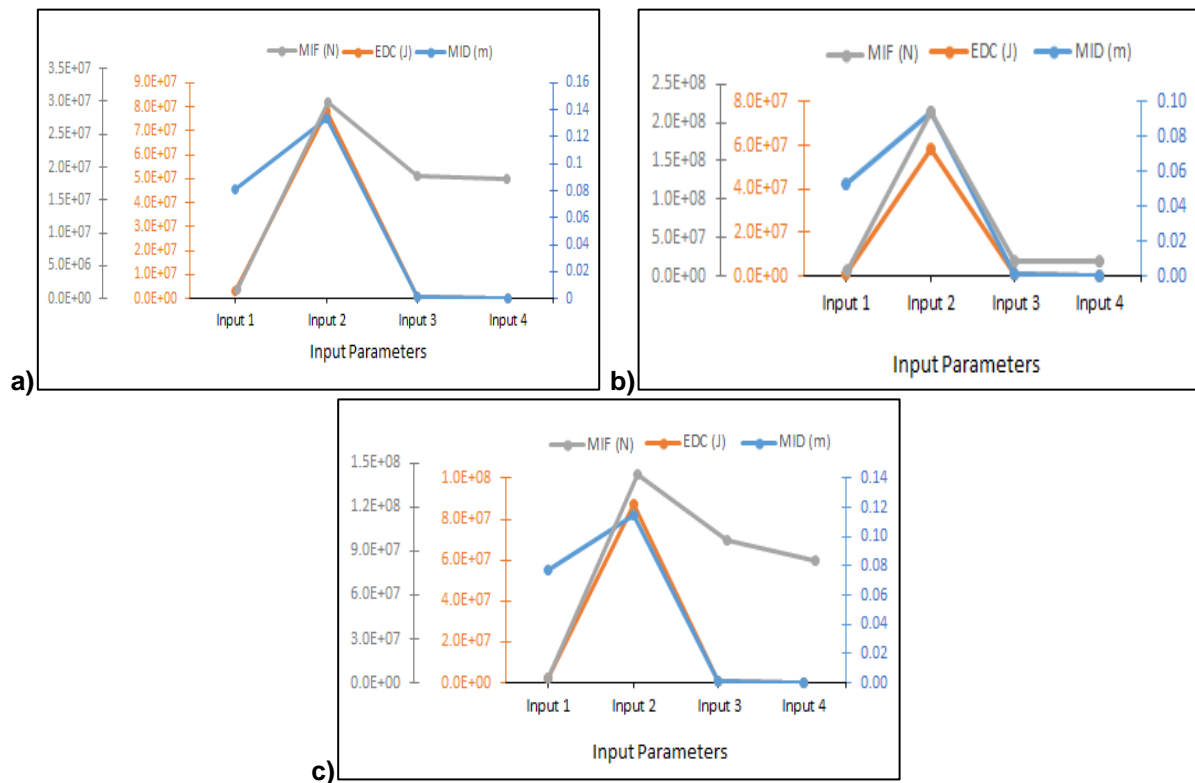| EARTHQUAKES		KOBE			DUZCE			ELCENTRO		
SLIDER TYPE		Eq.(12)	Eq.(13)	Eq.(14)	Eq.(12)	Eq.(13)	Eq.(14)	Eq.(12)	Eq.(13)	Eq.(14)
Input1	EDC (J)	3.25e6	1.29e6	1.99e6	3.02e6	7.34e5	1.85e6	5.39e5	4.00e5	4.72e5
	MIF (N)	1.45e6	7.66e6	2.79e6	1.47e6	5.90e6	2.69e6	1.15e6	3.58e6	1.63e6
	MID (m)	0.08	0.05	0.08	0.09	0.04	0.07	0.03	0.02	0.03
Input2	EDC (J)	7.84e7	5.84e7	8.72e7	6.02e7	2.74e7	4.62e7	5.13e7	2.30e7	3.61e7
	MIF (N)	2.98e7	2.14e8	1.42e8	2.67e7	1.34e8	8.47e7	2.39e7	8.08e7	6.13e7
	MID (m)	0.13	0.09	0.11	0.08	0.06	0.06	0.05	0.03	0.04
Input3	EDC (J)	6.97e5	6.95e5	6.15e5	4.26e5	4.24e5	3.39e5	9.95e5	9.92e5	8.30e5
	MIF (N)	1.85e7	7.99e7	9.73e7	1.87e7	2.03e7	1.08e8	1.86e7	1.92e7	6.28e7
	MID (m)	8.19e-4	8.18e-4	7.36e-4	0.001	0.001	8.4e-4	4.93e-4	4.92e-4	4.17e-4
Input4	EDC (J)	3.73e4	3.73e4	3.34e4	1.95e4	1.95e4	1.68e4	4.52e4	4.52e4	3.84e4
	MIF (N)	1.81e7	1.82e7	8.36e7	1.82e7	1.82e7	6.83e7	1.83e7	1.83e7	5.85e7
	MID (m)	6.70e-5	6.70e-5	6.09e-5	5.16e-5	5.15e-5	4.7e-5	4.16e-5	4.16e-5	3.77e-5

Looking at Fig. 11 and Table 5, Input 1 results in MID of approximately 0.03 m for both Equation (12) and (14), while for the same equations Input 2 results in MID of approximately 0.04 m under Elcentro. Additionally, Equation (13) results in approximately 0.02 and 0.03 m under Input 1 and 2, respectively. From this observation together with the observed base shear forces and base accelerations, Equation (13) can be the more effective than Equation (12) under Elcentro earthquake as it results in the smaller MID and reasonable $\ddot{U}_{b\max}$ under Input 1 and 2. Similar suggestions can

also be made for Duzce which is observed to result in MID of 0.09, 0.04 and 0.07 m under Input 1, and 0.08, 0.06 and 0.06 m under Input 2 for Equation (12), (13) and (14) respectively. Overall, curved slider defined by Equation (13) results in the smaller MID under Input 1 and 2, while flat slider results in the highest values followed by the proposed Equation (14) under all earthquakes, thus making Equation (13) the most reliable in terms of MID reduction under Inputs 1 & 2.
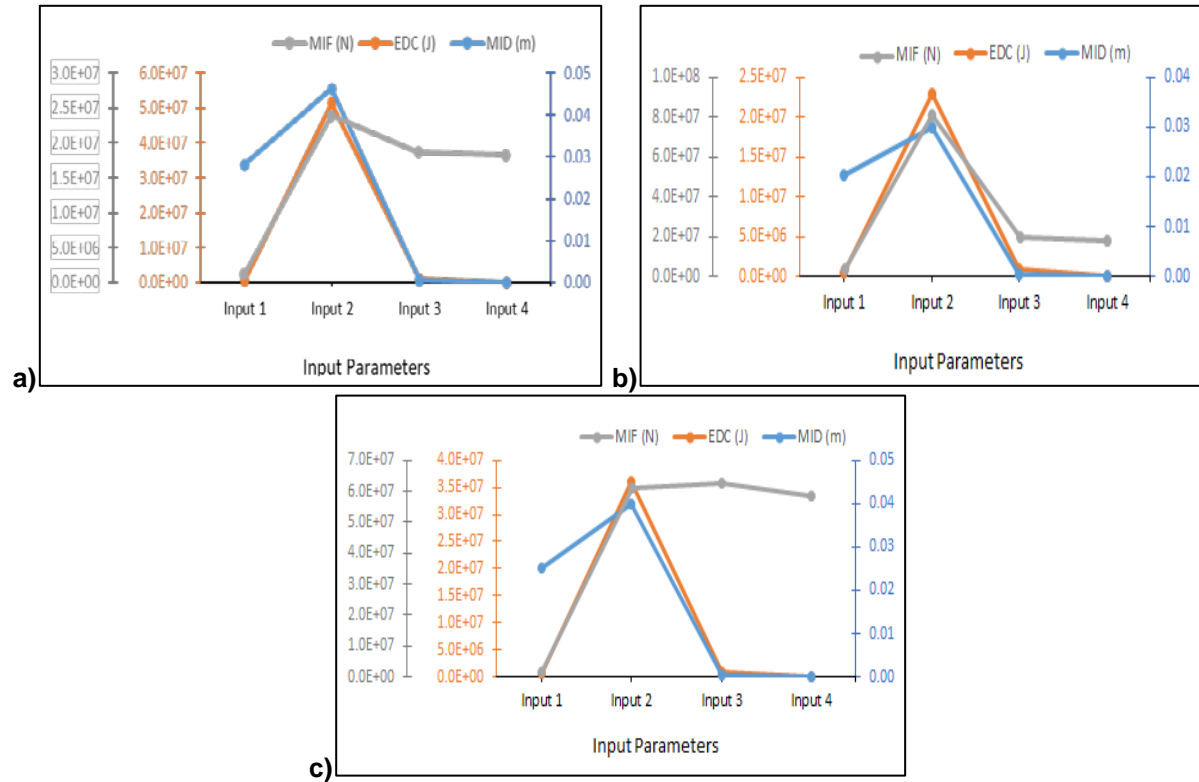
On the other hand, it can be seen that under Inputs 1, 2, 3 and 4, Kobe earthquake resulted in approximately 3,3,2,1.6; 2.6,2,1.6,1.6; and 3,3,1.8,1.6 times larger MID than Elcentro's under Equation (12), (13) and (14), respectively. Not surprisingly, strong earthquake results in higher MID than moderate earthquake as expected. Furthermore, as story stiffness increases, differences in MID from the two earthquakes become less pronounced; demonstrating that MID of conventional sliding bearings used to isolate stiffened superstructure may not significantly be affected by the earthquake magnitude.

Focusing on stiffened systems, Inputs 3 and 4 are observed to result in approximately equal values for both Equation (12) and (13) with nearly $8e^{-4}$ and $7e^{-5}$ m, respectively, whereas under Duzce nearly equal MID are observed for all equations of approximately 0.00005 and 0.001 m, respectively. On the other hand, under Elcentro these inputs result in approximately similar MID values of $4.9e^{-4}$ and $4.2e^{-5}$ m for Equation (12) and (13), while (14) results in slightly smaller MID of approximately $4.2e^{-4}$ and $3.8e^{-5}$ m under Inputs 3 and 4 respectively. These small displacements explain the inefficiency of the isolator to dissipate much energy, though their corresponding base floor accelerations and shear forces were observed to reduce significantly in Section 3.2. It is, therefore, necessary to mention that in situations where reduced base accelerations and shear forces are of first priority, stiffened superstructure can be adopted.

Kobe earthquake

a)

b)

c)

Elcentro earthquake

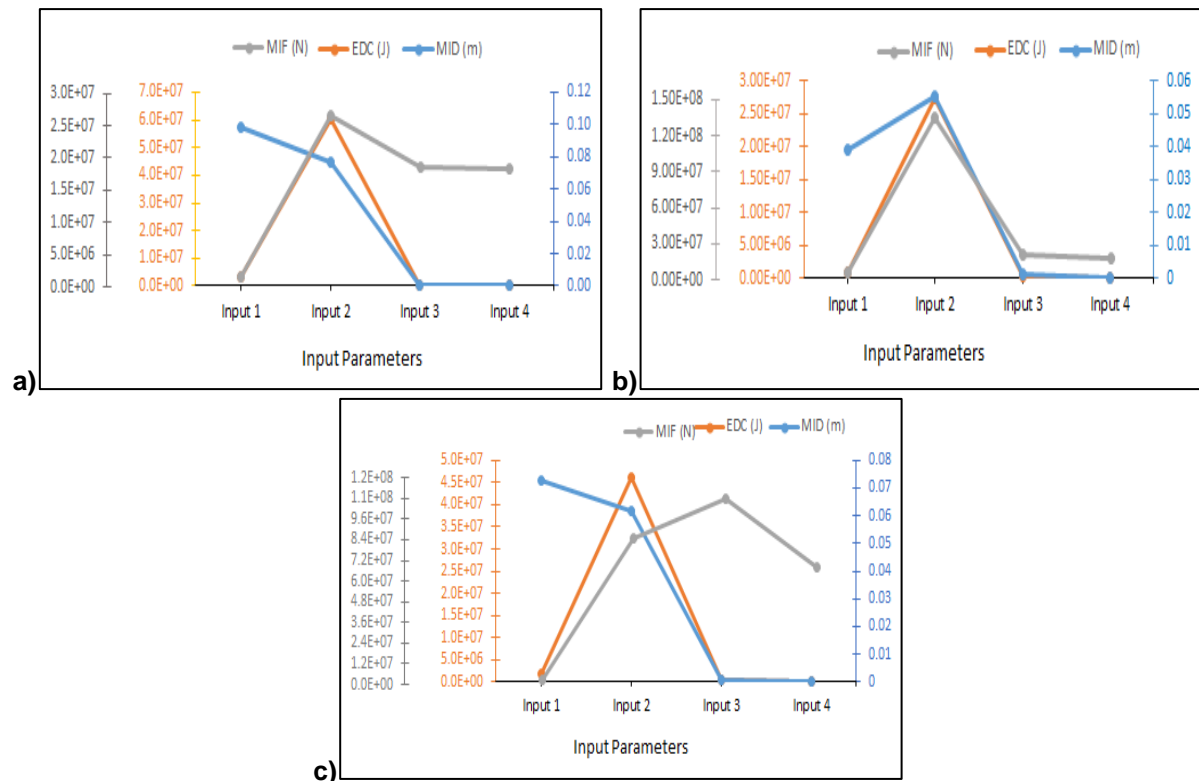

a)

b)

c)

Duzce earthquake

a)

b)

c)

Figure 11. Variation of EDC, MIF, and MID under Equations: a) (12), b) (13), c) (12).

Looking at the results of EDC, MIF, and MID in Fig. 11 under all inputs, all earthquakes tend to result in similar trends for each equation. Additionally, Equations (12) and (13) demonstrate that, for all types of earthquakes, the increase in superstructure stiffness decreases MIF to a certain value, thereafter levelling off such that further increase leads to negligible changes in MIF. The same holds for Equations (14) under Kobe and Elcentro, except under Duzce where an increase in MIF is observed as stiffness increases from Input 2 to 3, and further increase leading to decrease in MIF. Further observations show that increase in story stiffness leads to decrease in both MID and EDC for all

earthquakes as can be seen particularly considering Inputs 2, 3 and 4, where only story stiffness is increased while keeping the same story mass.

Overall, a comparative perspective from Fig. 11 demonstrates that Input 2 has higher EDC than Input 1 while the latter has smaller MIF, thus making the former possess desirable properties than the latter when dissipation is prioritized. Besides, both Input 1 and 2 can perform better as these inputs are capable of keeping EDC, MIF and MID responses in a comparable range while these responses from Inputs 3 and 4 are observed to alter significantly, with almost zero values of MID and EDC as can be seen in Fig.11 and Table 5.

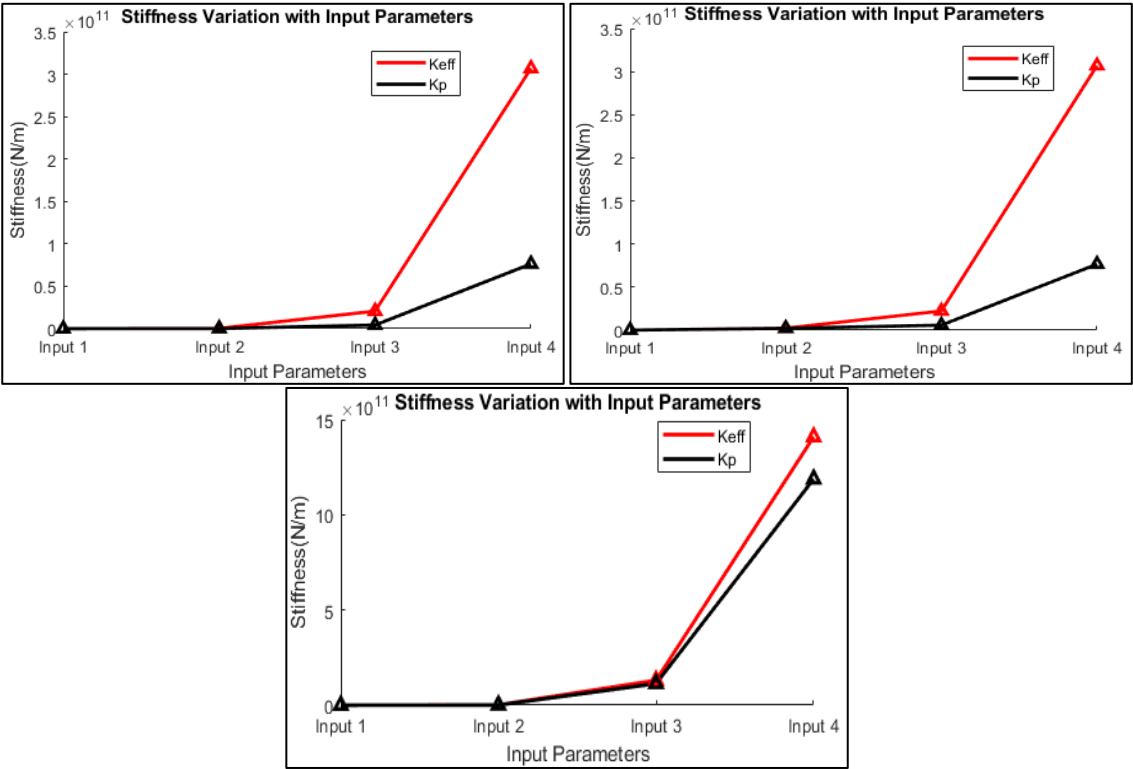### 3.5. Effective and Post-yield Stiffness

In order to maintain the hysteretic behavior of the bearing and define the isolation period in such a way that resonance is avoided, it is important to control the stiffness of the isolator. Effective stiffness $\left(K_{eff} \right)$ and post-yield stiffness $\left(K_p \right)$ of the isolator are compared for each input and equation to provide insights on the behavior of isolator in terms of its consistency in keeping desirable hysteretic behavior under horizontal loading. Looking at the isolator stiffness variation under Kobe earthquake, it can be seen from Table 6 and Fig. 12 that Input 1 results in K_{eff} and K_p of approximately 1.65e7 and 7.69e6, 1.45e8 and 1.38e8, and 3.62e7 and 2.65e7 N/m; while K_{eff} and K_p under Input 2 are 2.38e8 and 1.17e8, 2.28e9 and 2.15e9, and 1.25e9 and 1.13e9 N/m, for Equation (12), (13) and (14), respectively.

Table 6. Effective and post-yield stiffness under various sliding bearings and earthquakes.
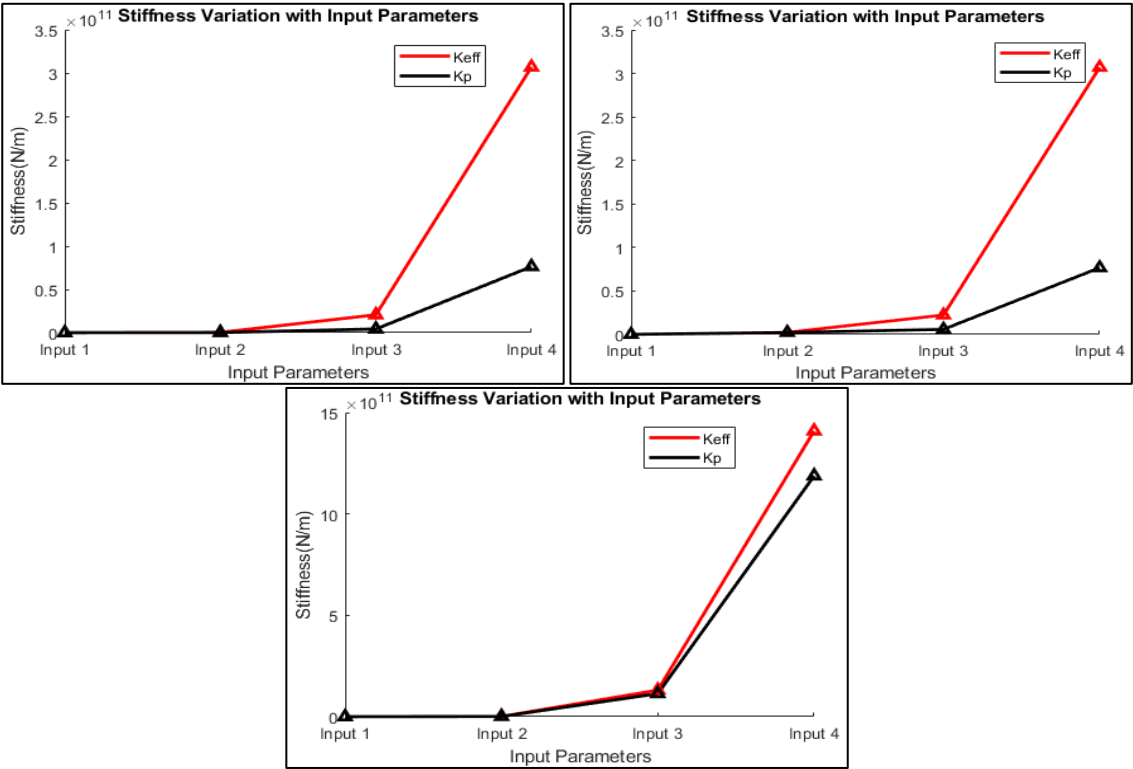
EARTHQUAKES		KOBE			DUZCE			ELCENTRO		
TYPE OF SLIDERS		Eq.(12)	Eq.(13)	Eq.(14)	Eq.(12)	Eq.(13)	Eq.(14)	Eq.(12)	Eq.(13)	Eq.(14)
Input1	K_{eff}	1.65e7	1.45e8	3.62e7	1.47e7	1.47e8	3.63e7	3.62e7	1.74e8	6.07e7
	K_p	7.69e6	1.38e8	2.65e7	6.51e6	1.44e8	2.68e7	1.22e7	1.67e8	3.66e7
Input2	K_{eff}	2.38e8	2.28e9	1.25e9	3.47e8	2.42e9	1.37e9	4.99e8	2.68e9	1.53e9
	K_p	1.17e8	2.15e9	1.13e9	1.62e8	2.21e9	1.17e9	2.12e8	2.31e9	1.22e9
Input3	K_{eff}	2.39e10	2.57e10	1.33e11	2.07e10	2.23e10	1.31e11	4.20e10	4.34e10	1.56e11
	K_p	5.15e8	6.88e9	1.15e11	4.27e9	5.92e9	1.14e11	8.79e9	1.01e10	1.20e11
Input4	K_{eff}	3.14e11	3.15e11	1.42e12	3.07e11	3.07e11	1.41e12	5.46e11	5.49e11	1.67e12
	K_p	5.67e10	5.86e10	1.16e12	7.64e10	7.67e10	1.19e12	9.63e10	9.64e10	1.21e12

With similar interpretation as above for other earthquakes, it can be observed that K_p is consistently less than K_{eff} as expected for all equations and earthquakes. Additionally, both K_p and K_{eff} are observed to increase as the stiffness of the superstructure increases. Thus, Input 1 has the least values of K_{eff} and K_p due to its lowest superstructure stiffness while Input 4, which has the highest superstructure stiffness, has the highest isolator stiffness.

Duzce earthquake

Kobe earthquake

Dushimimana, A., Singirankabo, E., Kathumbi, L.K.
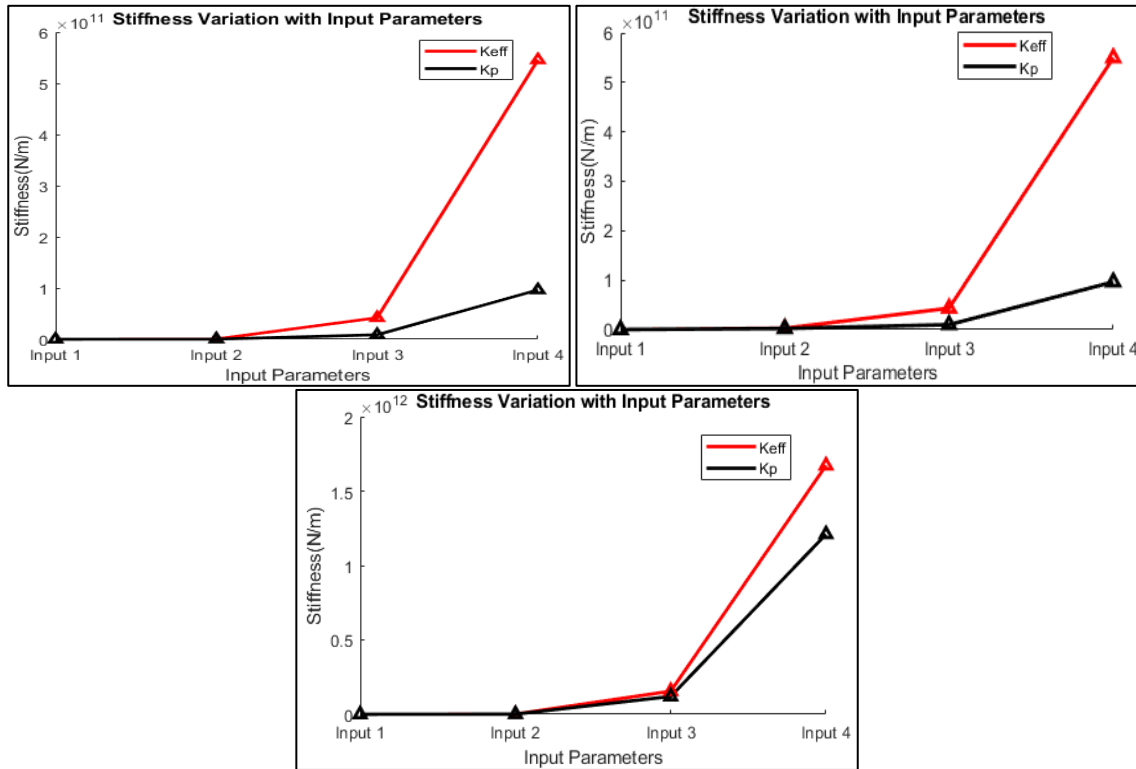
Elcentro earthquake

Figure 12. Effective and post-yield stiffness variation under various bearings and inputs.

The above observations are in agreement with the previously observed isolator displacement trends, which are found to be smaller for Inputs 4 and 3 compared to other inputs due to the presence of very high K_{eff} and K_p that prevent and limit the isolator flexibility, and hence leading to small MID. It is, furthermore, of paramount importance to indicate that this prevention of isolator flexibility results in small EDC as previously discussed. Under all studied earthquakes and inputs, it is also important to note that Equation (12) results in the smallest K_{eff} and K_p, followed by Equation (14) and Equation (13), respectively. This makes flat surface slider possess the best performance in terms of minimizing K_{eff} and K_p, as well as providing desirable MIDs, followed by curved slider defined by Equation (14) and lastly by (13). This shows again that Equation (14) can be more effective than (13) in terms of isolator stiffness control, particularly for stiffened superstructure where the proposed equation has previously shown tremendous behavior over the existing equation (13). On the other hand, comparing Elcentro results with Kobe's, it can be seen that the latter earthquake results in smaller stiffness values indicating that NF earthquakes will lead to larger MID, owing to their ability to reduce the isolator stiffness as compared to moderate earthquakes like Elcentro. Furthermore, authors in [46] reported that high isolator stiffness can increase superstructure accelerations for NF earthquake, and high post-yield stiffness leads to limited lateral displacement capacity [45], which is in agreement with the observed increased acceleration under Kobe earthquake when Input 2 (which results in higher isolator stiffness than Input 1) is adopted, hence showing the importance of controlling the isolator effective and post-yield stiffness.

3.6. Superstructure Story Drifts, Shears and Accelerations

Typical story drifts, peak story acceleration and shears are shown in Table 7 for Input 2. It can be seen that the maximum story drifts occur at the first story as previously reported by Hassan and Pal [48]. Furthermore, peak story accelerations are observed to be similar for all investigated equations, and found to be reduced by approximately 34, 50, and 39 % (in comparison with fixed base structure) under Kobe, Duzce and Elcentro, respectively. Similar reductions are also observed in terms of peak story shear forces as can be seen in Table 7. From this observation, conventional sliding bearings can have their best performance under earthquakes with NF such as Duzce (with small PGV) and LP moderate like Elcentro, outlining that behavior of these bearings is significantly influenced by the type of earthquakes.

Table 7. Peak story acceleration and shear, and story drifts.

Slider		Kobe Earthquake			Duzce Earthquake			Elcentro Earthquake		
		Eq.(12)	Eq.(13)	Eq.(14)	Eq.(12)	Eq.(13)	Eq.(14)	Eq.(12)	Eq.(13)	Eq.(14)
PSA (%)			33.699			50.303			38.964	
PSF (%)			33.676			50.303			38.965	
	SD1	0.12	0.14	0.18	0.13	0.09	0.10	0.08	0.05	0.07
	SD2	0.06	0.06	0.06	0.03	0.03	0.03	0.02	0.02	0.02
	SD3	0.07	0.07	0.07	0.03	0.03	0.03	0.02	0.02	0.02
	SD4	0.06	0.06	0.06	0.04	0.04	0.04	0.02	0.02	0.02
Input2	SD5	0.06	0.06	0.06	0.04	0.04	0.04	0.02	0.02	0.02
	SD6	0.08	0.08	0.08	0.02	0.02	0.02	0.02	0.02	0.02
	SD7	0.07	0.07	0.07	0.01	0.01	0.01	0.02	0.02	0.02
	SD8	0.07	0.07	0.07	0.05	0.05	0.05	0.02	0.02	0.02
	SD9	0.05	0.05	0.05	0.04	0.04	0.04	0.02	0.02	0.02
	SD10	0.04	0.04	0.04	0.02	0.02	0.02	0.01	0.01	0.01

Abbreviations: PSA, PSF are peak story acceleration and shear forces respectively, SD: story drift

4. Conclusion

In this study, effectiveness of conventional sliding bearings (flat and curved surface sliders) as seismic-isolators was examined. The study also attempted to improve the existing equation for curved sliding bearing by directly relating the isolator stiffness to the first story stiffness of the investigated structure. Four different input parameters reflecting the superstructure stiffness variation were adopted for a 10 story RC structure model isolated by flat and curved bearings and its structural responses were examined under LP moderate and strong NF earthquake ground motions. To achieve this, Full Structural Response Investigation (FSRI) was applied as a new and desirable strategy to fully investigate the behavior of isolated structures when exposed to seismic-loads, as this can provide a whole picture of the isolated structure behavior. Key findings after applying the FSRI are as follows:

1. All investigated bearings perform similarly and equally in reducing U_{top} for each used Input.

U_{top} is smaller when moderate earthquake is used than when strong one is adopted, though the nature of Duzce (with smaller PGV than Kobe's) makes it behave as Elcentro, indicating that earthquake's PGV (along with PGA) needs consideration when investigating seismic isolation systems. Increase in stiffness leads to decrease in U_{top}, and all the earthquakes tend to result in approximately similar displacement profiles for stiffened superstructure, indicating that for such superstructure the U_{top} may not significantly be affected by the earthquake type. Flat surface slider can be the best in U_{top} control for less stiffened superstructure. On the other hand, both flat and curved bearings are observed to possess equal ability in reducing peak story accelerations and shear forces, and in keeping similar story drifts, except for the first story where moderate Duzce earthquakes tend to render curved slider performance better.

2. Stiffening of superstructure can lead to reduction of base shear forces and accelerations, but affect the bearing flexible, hence causing small isolator displacements, which lead to less EDC. This provides insights about how setting priorities during design is vital as seismic isolation may not be able to provide all desirable FSRI responses. For example, in situations where $\ddot{U}_{b\max}$ reduction and increased EDC are of first priority (rather than reduced U_{top}), equal stiffness for all floors can be adopted for the investigated bearings, as varied story stiffness leads to amplification of $\ddot{U}_{b\max}$ despite of its best performance in reducing U_{top} Furthermore, curved surface slider results in the smallest $\ddot{U}_{b\max}$ for all earthquakes, thus making it the most effective in reducing $\ddot{U}_{b\max}$.

3. Strong NF earthquakes are found to result in higher MID than LP moderate earthquake as expected. As story stiffness increases, differences in MID from both earthquakes become less pronounced. This demonstrates that MID of conventional sliding bearings may not significantly be affected by the earthquake magnitude when the superstructure is stiffened. Focusing on the observed

TIs, type of earthquake and Input parameters are observed to significantly affect TIs, hence should be examined when investigating the performance of seismic isolation systems.

4. Having a comparative perspective on the results of EDC, MIF, MID under all Inputs, all earthquakes tend to result in similar trends for each slider. Additionally, results from flat and curved sliders demonstrate that the increase in superstructure stiffness decreases MIF to a certain value thereafter levelling off so that further increase leads to negligible changes in MIF. The same holds for the proposed formula under Kobe and Elcentro, except under Duzce where an increase in MIF is observed as stiffness increases from Input 2 to 3, and further increase leading to decrease in MIF. Flat surface slider is found less reliable in terms of MID reduction under Inputs 1&2, though it is observed to perform better in terms of EDC increase and MIF reduction. Therefore, in situations where reduced MID is prioritized, curved slider has more beneficial effects.

5. K_p is observed to be consistently less than K_{eff} as expected under all equations and earthquakes, and both increase as the superstructure stiffness increases. Flat surface slider results in the smallest K_{eff} and K_p rendering it the most effective. Furthermore, the proposed formula can be more effective in terms of isolator stiffness control, particularly for stiffened superstructure. Using similar story stiffness under Duzce and Elcentro result in unwanted long-lasting U_{top} peaks over nearly the entire duration of each earthquake, which can cause substantial damage of sensitive equipment in the building.

6. The formulated equation is tested and found reliable only when the superstructure is stiffened, owing to its conservative behavior over a wide range of superstructure stiffness, and ability in controlling seismic isolation responses. In this case, this equation can even perform much better than the existing Equation, which underestimates isolator stiffness due to its conservative inability. On the other hand, flat surface slider can have better performance than the curved one, when less stiffened superstructure is adopted, and comparable performance, when superstructure stiffness increases.

References

1. Han, Q., Wen, J., Lin, L., Jia, J. Experimental and numerical studies on multi-spherical sliding friction isolation bearing. Journal of Vibroengineering. 2014. 16 (5). Pp. 2394–2405.

2. Saitta, F., Clemente, P., Buffarini, G., Bongiovanni, G., Salvatori, A., Grossi, C. Base Isolation of Buildings with Curved Surface Sliders : Basic Design Criteria and Critical Issues. Advances in Civil Engineering. 2018. 2018. DOI: 10.1155/2018/1569683.

3. Yang, T., Eeri, M., Calvi, P.M., Eeri, M., Wiebe, R. Numerical implementation of variable friction sliding base isolators and preliminary experimental results. earthquake Spectra. 2020. Pp. 1–21. DOI: 10.1177/8755293019891721

4. Weber, F., Obholzer, F., Huber, P., Hartinger, M., Meier, L., Distl, J., Braun, C. New Adaptive Curved Surface Slider for Enhanced Structural Isolation, Reduced Displacement Capacity. 16th European Conference on Earthquake Engineering. 2018. (18-21 June).

5. Shahabi, A.B., Ahari, G.Z., Barghian, M. Base Isolation Systems – A State of the Art Review According to Their Mechanism. Journal of Rehabilitation in Civil Engineering. 2020. 2 (8). Pp. 37–61. DOI: 10.22075/JRCE.2019.16186.1306

6. Kasimzade, A.A., Dushimimana, A., Tuhta, S., Atmaca, G., Günday, F., Pfidze, K., Abrar, O. A Comparative Study on Effectiveness of Using Horasan Mortar as a Pure Friction Sliding Interface Material. European Journal of Engineering Research and Science. 2019. 4 (2). Pp. 20–24. DOI: 10.24018/ejers.2019.4.2.1166.

7. Mokha, A.S., Constantinou, M.C., Reinhorn, A.M. Verification of Friction Model of Teflon Bearings under Triaxial Load. Journal of Structural Engineering. 1993. 119 (1). Pp. 240–261.

8. Mokha, B.A., Constantinou, M., Member, A., Reinhorn, A. Teflon bearings in base isolation. 1: Testing. Journal of Structural Engineering. 1990. 116 (2). Pp. 438–454. DOI: 10.1061/(asce)0733-9445(1990)116:2(438)

9. Lago, A., Trabucco, D., Wood, A. An introduction to dynamic modification devices. Damping Technologies for Tall Buildings. Butterworth-Heinemann. Chicago, 2018.

10. Castellano, M.G., Colato, G.P., Infanti, S., Borella, R. Seismic isolation of continuous bridges through curved surface sliders combined with shock transmission units. WCEE. 2012.

11. Tyler, G.R. Dynamic Tests on PTFE Sliding Layers under Earthquake Conditions. Bulletin of the New Zealand and National Society for Earthquakes Engineering. 1977. 10 (3).

12. Cimellaro, G.P., Nagarajaiah, S., Kunnath, S.K. Computational Methods, Seismic Protection, Hybrid Testing and Resilience in Earthquake Engineering. Springer Cham Heidelberg. New York, 2015.

13. Scheaua, F.D. Friction Pendulum Dampers for Earthquake Isolated Structural Systems. Engineering Faculty of Braila. 2012. URL: https://www.researchgate.net/publication/292174529%0AFriction

14. Constantinou, M.C., Whittaker, A.S., Kalpakidis, Y., Fenz, D.M., Warn, G.P. Performance of Seismic Isolation Hardware under Service Siesmic Loading New York, 2007.

15. Kumar, M., Whittaker, A.S., Constantinou, M.C. Characterizing friction in sliding isolation bearings. Earthquake Engineering & Structural Dynamics. 2015. 44 (November 2014). Pp. 1409–1425. DOI: 10.1002/eqe

16. Zayas, V.A. Earthquake Protection Column Support. United States Patent. Calofonia, 1987.

17. Zayas, V., Low, S.S., Mahin, S.A. The FPS earthquake resisting system, experimental reportSan Francisco, CA, 1987.

Dushimimana, A., Singirankabo, E., Kathumbi, L.K.

18. Gandelli, E., Quaglini, V. Effect of the Static Coefficient of Friction of Curved Surface Sliders on the Response of an Isolated Building. Journal of Earthquake Engineering. 2018. 00 (00). Pp. 1–29. DOI: 10.1080/13632469.2018.1467353.

19. Xu, Y., Guo, T., Yan, P. Design optimization of triple friction pendulums for base-isolated high-rise buildings. 2019. DOI: 10.1177/1369433219849840

20. Mokha, A., Constantinou, M.C., Reinhorn, A.M., Zayas, V.A. Experimental Study of Friction-Pendulum Isolation System. Journal of Structural Engineering. 1991. 9445 (November 1991). Pp. 3315–3336. DOI: 10.1061/(ASCE)0733-9445(1991)117

21. Fenz, D.M., Constantinou, M.C. Behaviour of the double concave Friction Pendulum bearing. 2006. (June). Pp. 1403–1424. DOI: 10.1002/eqe

22. Fenz, D.M., Eeri, S.M., Constantinou, M.C., Eeri, M. Modeling Triple Friction Pendulum Bearings for Response-History Analysis. Earthquake engineering practice. 2008. 24 (4). Pp. 1011–1028. DOI: 10.1193/1.2982531

23. Xu, Y., Guo, T., Yan, P. Design optimization of triple friction pendulums for base-isolated high-rise buildings. Advances in Structural Engineering. 2019. Pp. 1–14. DOI: 10.1177/1369433219849840

24. Moeindarbari, H., Taghikhany, T. Seismic optimum design of triple friction pendulum bearing subjected to near-fault pulse-like ground motions. Struct. Multidisc Optim. 2014. DOI: 10.1007/s00158-014-1079-x

25. Fadi, F., Constantinou, M.C. Evaluation of simplified methods of analysis for structures with triple friction pendulum isolators. Earthquake Engineering & Structural Dynamics. 2010. 39. Pp. 5–22. DOI: 10.1002/eqe

26. Namiranian, P., Amiri, G.G., Veismoradi, S. Near-fault seismic performance of triple variable friction pendulum bearing. Journal of Vibroengineering. 2016. 19 (4). Pp. 2293–2303. DOI: 10.21595/jve.2015.16280. URL: http://dx.doi.org/10.21595/jve.2015.16280

27. Xu, Y., Guo, T., Asce, M., Yan, P., Li, A. Effect of Semiactive Control on Wind and Seismic Responses of High-Rise Building Supported on Triple Friction Pendulums. American Society of Civil Engineers. 2020. 34 (3). DOI: 10.1061/(ASCE)CF.1943-5509.0001427

28. Design, L., Wen, J., Han, Q., Du, X. Shaking table tests of bridge model with friction sliding bearings under bi-directional earthquake excitations. Structure and Infrastructure Engineering. 2019. 15 (9). Pp. 1264–1278. DOI: 10.1080/15732479.2019.1618350. URL: https://doi.org/10.1080/15732479.2019.1618350

29. Lee, D., Constantinou, M.C. Quintuple Friction Pendulum Isolator Behavior, Modeling and Validation New York, 2015.

30. Poornima, B.S., Babu, B.S.J. Comparative Study on Seismic Response of Regular and Irregular RC Framed Buildings with HDRB, LRB and FPS Base Isolation Systems. International Journal for Research in Applied Science & Engineering Technology. 2019. 7 (Vi). Pp. 805–813.

31. Pokhrel, A., Jianchun, L., Yancheng, L., Maksis, N., Yu, Y. Comparative Studies of Base Isolation Systems featured with Lead Rubber Bearings and Friction Pendulum Bearings. Applied Mechanics and Materials. 2016. 846. Pp. 114–119. DOI: 10.4028/www.scientific.net/AMM.846.114

32. Tsopelas, P., Nagarajaiah, S., Constantinou, M.C., Reinhorn, A.M. 3D-BASIS-M : Nonlinear Dynamic Analysis of Multiple Building Base Isolated Structures. 1991.

33. Hur, D., Hong, S.-C. Analysis of an Isolation System with Vertical Spring-viscous Dampers in Horizontal and Vertical Ground Motion. Applied Sciences. 2020. 10 (1411). DOI: 10.3390/app10041411

34. Dushimimana, A., Niyonsenga, A.A., Decadjevi, G.J., Kathumbi, L.K. Effects of model-based design and loading on responses of base-isolated structures. Magazine of Civil Engineering. 2019. 92 (8). Pp. 141–153. DOI: 10.18720/MCE.92.12

35. University of California. Pacific Earthquake Engineering Research Center (PEER) NGA: Ground Motion Database. 2013.

36. Gunday, F., Dushimimana, A., Tuhta, S. Analytical and Experimental Modal Analysis of a Model Steel Structure Using Blast Excitation. International Conference on Innovative Engineering Application (CIEA2018). 2018. Pp. 686–694.

37. Dushimimana, A., Günday, F., Tuhta, S. Operational Modal Analysis of Aluminum Model Structures using Earthquake Simulator. International Conference on Innovative Engineering Application (CIEA2018). 2018. Pp. 677–685.

38. Dushimimana, A., Ziada, M., Tuhta, S. Effect of Carbon Fiber Reinforced Polymer (CFRP) Composites Applied to Walls and Slabs of Masonry Building. International Journal of Advance Engineering and Research Development. 2018. 5 (04l). Pp. 2348–4470. DOI: 10.21090/IJAERD.76958

39. Sena-cruz, J., Correia, L., Ribeiro, F., Figueira, D., Benzo, P.G., Barros, J., Pereira, E., Valente, I. The effect of surface treatment and environmental actions on the adhesive connection between GFRP laminate surface and fresh FRC. Construction and Building Materials. 2020. 258. DOI: 10.1016/j.conbuildmat.2020.119594

40. Correia, L., Sena-Cruz, J., Michels, J., França, P., Pereira, E., Escusa, G. Durability of RC slabs strengthened with prestressed CFRP laminate strips under different environmental and loading conditions. Composites Part B. 2017. DOI: 10.1016/j.compositesb.2017.05.047. URL: http://dx.doi.org/10.1016/j.compositesb.2017.05.047

41. Ebadi, P., Farajloomanesh, S. Seismic design philosophy of special steel plate shear walls. Magazine of Civil Engineering. 2020. 95 (3). Pp. 3–18. DOI: 10.18720/MCE.95.1

42. Jain, S.K., Thakkar, S.K. Application of base isolation for flexible buildings. 13th World Conference on Earthquake Engineering. 2004. Pp. 1924.

43. Belash, T.A., Ivanova, Z.V. Timber frame buildings with efficient junction designs for earthquake-prone areas. Magazine of Civil Engineering. 2019. 92 (8). Pp. 84–95. DOI: 10.18720/MCE.92.7

44. Dushimimana, A., Nzamurambaho, F., Shyaka, E., Niyonsenga, A.A. Optimum Performance of Isolation System for Medium Rise Buildings Subject to Long Period Ground Motions. International Journal of Applied Engineering Research. 2018. 13 (23). Pp. 16342–16350.

45. Dicleli, M. Supplemental elastic stiffness to reduce isolator displacements for seismic-isolated bridges in near-fault zones. Engineering Structures. 2007. 29. Pp. 763–775. DOI: 10.1016/j.engstruct.2006.06.013

46. Matsagar, V.A., Jangid, R.S.Ã. Influence of isolator characteristics on the response of base-isolated structures. Engineering Structures. 2004. 26 (12). Pp. 1735–1749. DOI: 10.1016/j.engstruct.2004.06.011

47. Dicleli, M., Karalar, M. Optimum characteristic properties of isolators with bilinear force – displacement hysteresis for seismic protection of bridges built on various site soils. Soil Dynamics and Earthquake Engineering. 2011. 31 (7). Pp. 982–995. DOI: 10.1016/j.soildyn.2011.03.005. URL: http://dx.doi.org/10.1016/j.soildyn.2011.03.005

48. Hassan, A., Pal, S. Effect of soil condition on seismic response of isolated base buildings. International Journal of Advanced Structural Engineering. 2018. 10 (3). Pp. 249–261. DOI: 10.1007/s40091-018-0195-z. URL: https://doi.org/10.1007/s40091-018-0195-z

Contacts:

Aloys Dushimimana, chenkodu432 @gmail.com

Lilies Kathami Kathumbi, 06lilies @gmail.com

Edouard Singirankabo, nkabo12edus @gmail.com